Electronic Supplementary Information (ESI)

Photoreaction-Driven Two-Dimensional Periodic Polyrotaxane-type Supramolecular Nanoarchitecture

Cai-Cai Zhang,[a] Ying-Ming Zhang,[a] Zhi-Yuan Zhang,[a] Xuan Wu,[a] Qilin Yu[a] and Yu Liu[a,b*]

[a]Department of Chemistry, State Key Laboratory of Elemento-Organic Chemistry, Nankai University, Tianjin 300071, P. R. China.

[b]Collaborative Innovation Center of Chemical Science and Engineering (Tianjin), Nankai University, Tianjin 300071, P. R. China

[*]Address correspondence to yuliu@nankai.edu.cn

Contents

1、General information. 3

2、Synthetic procedures. 5

3、Characterization of TPA-SP and M-SP. 8

4、Characterization of TPA-SP⊂CB[8] complex. 14

5、Characterization of TPA-SP_{PD}⊂CB[8]. 26

6、Characterization of C_{60}@(TPA-SP_{PD}⊂CB[8]). 30

7、Effects of the C_{60}@(TPA-SP_{PD}⊂CB[8]) on ROS generation. 34

8、References 34

1□ General information.

Materials and methods

All chemicals were commercially available unless noted otherwise. NMR spectroscopy was recorded on a Brucker AV400 spectrometer. High resolution mass spectra were performed on Varian 7.0T FTMS. Low resolution mass spectra were performed on LCQ-Adantage. UV/vis spectra were recorded on Thermo Scientific EVOLUTION 300 spectrophotometer equipped with a HAAKE SC 100 temperature controller to keep the temperature at 25 °C. DLS data were collected on a laser light scattering spectrometer (BI-200SM) equipped with a digital correlator (Turbo Corr) at 636 nm at a scattering angle of 90°. The solutions of CB[8] and TPA-SP were passing a 0.25 μm syringe filter, respectively, and then mix them together in proportion. The samples for TEM measurement were prepared by dropping the solution onto copper grids and then air-dried. The samples were examined by FEI/Tecnai G2 F20 microscope equipped with a CCD camera (Orius 832, Gatan) operating at an accelerating voltage of 200 keV. Atomic force microcopy was carried out with a Nanoscope IIIa Multimode 8 AMF. The samples were prepared by dropping the solution onto mica and then air-dried. Scanning electron microscopy was performed on ZEISS Merlin Campact scanning electron microscope. The samples were prepared by dropping the solution onto silicon wafer and then air-dried. Grazing incidence small angle X-ray scattering (GI-SAXS) measurement was performed on Rigaku Smart Lab equipped with a Cu Kα radiation source (λ = 0.1542 nm). Fourier transform infrared spectroscopy was carried out with a Bruker TENSOR II FT-IR

spectrometer. Surface area measurements were conducted on a Quantachrome instruments. Each sample was degassed at 110 °C for 12 h and then backfilled with N_2. Surface parameters were determined using Multi-point BET. Thermogravimetric analysis (TGA) was performed on a NETZSCH STA449F3 form room temperature to 700 °C at the heating rate of 10 °C/min under N_2.The pH of the solution was measured with Thermo Scientific Orion Start A211. The glass electrode was calibrated at pH 4, 7, 10 with buffer standards.The light irradiation experiments were performed using a 300W Xe lamp (CEL-HXF300 14V) with optical filter; 365 nm light irradiation experiments were carried out by a portable ultraviolet lamp. Agarose gels of 1% were prepared by heating 250 mg of agarose in 25 mL of TAE buffer. Solutions containing pBR322 DNA and samples were prepared by adding an appropriate volume of samples and DNA solutions into Eppendorf tubes and then were diluted to the total volume of 10 μL. After incubation by white light (420–700 nm band pass filter) irradiation or in the dark, the solutions were subjected to electrophoresis at 60 V for 45 min (current 120 mA).

Cell death assay

A549 cells were seeded in 96-well plates (5×10^4 cells mL^{-1}, 100 μL per well) for 24 h at 37 °C in 5% CO_2. Then, the cells were incubated with the complex at different concentrations ([TPA-SP] = 0, 2, 4, and 8 μM, respectively) for 12 h, respectively. After irradiation with white light source (420–700 nm band pass filter) for 10 min, the cells were incubated for another 12 h. Then the cells stained by propidium iodide (PI,

5 μg/mL) for 5 min, and then observed by confocal microscopy (FV1000, Olympus, Japan). The total cells and PI-positive cells were counted by ImageJ software, and the percent of PI-positive cells were calculated. All data presented as the mean ± standard deviation.

Measurement of intracellular reactive oxygen species (ROS)

A549 cells were treated with the complex at the indicated concentrations for 24 h and then incubated with 20 μg/ml DCFH-DA in F12 medium for 15 min at 37 °C in the dark. The fluorescence intensity of the cells was measured immediately with excitation at 480 nm and emission at 520 nm.

2、Synthetic procedures.

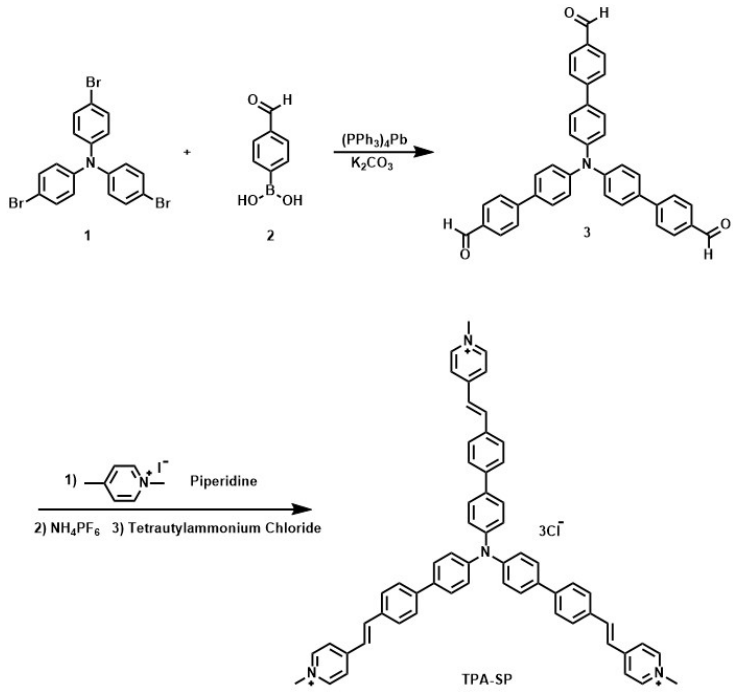

Scheme S1. The route of synthesis of TPA-SP.

Synthesis of **3**[S1]

Tris(4-bromophenyl)amine (4.82 g, 10 mmol) and 4-formylphenylboronic acid (5.99 g, 40

mmol) were dissolved in 150 mL dioxane. Aqueous solution of K_2CO_3 (11.05 g, 80 mmol) was added into the dioxane solution under N_2 atomosphere. After the addition of $(PPh_3)_4Pd$ (577.70 mg 0.5 mmol) to the degassed mixed solution with vigorous stirring under N_2, the system was refluxed for 48 hours. The solution was extracted with dichloromethane three times. The obtained organic layer was washed with water and brine, and then dried with $MgSO_4$. The resulting crude product was purified by column chromatography using silica gel (5.02 g, 90%). ^{1}H NMR (400 MHz, d_6-DMSO, 25 °C) δ 10.04 (s, 3H), 7.99 (d, J = 8.4 Hz, 6H), 7.92 (d, J = 8.4 Hz, 6H), 7.80 (d, J = 8.7 Hz, 6H), 7.24 (d, J = 8.7 Hz, 6H). ^{13}C NMR (100 MHz, d_6-DMSO, 25 °C) δ 192.62, 146.94, 145.07, 134.72, 133.45, 130.20, 128.44, 126.77, 124.38.

Synthesis of **TPA-SP**

Compound 3 (1.67g, 3 mmol) and 1,4-dimethylpyridiniumiodide (2.54g 10.8 mmol) were added in 50 mL methanol, and then drops of piperidine were added as catalyst. The solution was heated at 60 ℃ for 12 hours. After cooling down, lots of precipitate was collected by filtration, recrystallized with methanol several times, resulting in red solid. Dissolve the solid in a minimum amount of water, and then 1.46 g NH_4PF_6 was added. After a while, a plenty of precipitate appeared, filtered and washed the precipitate with lots of water to get orange solid. Subsequently, the solid was dissolved into 50 mL acetonitrile, 2.50 g tetrabutylammonium chloride was added, and then red precipitate appeared, filtered and washed with lots of acetonitrile to get red solid. Dried under vacuum, red powder was obtained (2.37g, 85%). ^{1}H NMR (400 MHz, d_6-DMSO, 25 °C) δ 8.88 (d, J = 6.6 Hz, 6H), 8.24 (d, J = 6.5 Hz, 6H), 8.07 (d, J = 16.3 Hz, 3H), 7.85 (s, 12H), 7.81 (d, J = 8.6 Hz, 6H), 7.58 (d, J = 16.2 Hz, 3H), 7.23

(d, J = 8.5 Hz, 6H), 4.26 (s, 9H). ^{13}C NMR (100 MHz, d_6-DMSO, 25 °C) δ 152.45, 146.60, 145.07, 141.09, 140.15, 133.90, 133.78, 128.83, 127.92, 126.72, 124.30, 123.46, 123.04, 46.88. HRMS (ESI) for $C_{60}H_{51}N_4Cl_3$: calcd. $[M\text{-}3Cl]^{3+}/3$: 275.8038, found: 275.8035. Melting point: 212 °C.

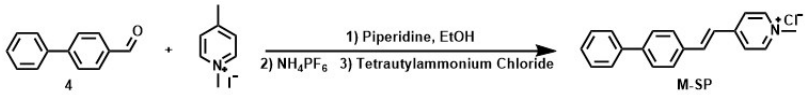

Scheme S2. The route of synthesis of M-SP.

Synthesis of **M-SP**

Similar synthesis method to TPA-SP. Dried under vacuum, yellow powder was obtained and the yeild is 87%.

^{1}H NMR (400 MHz, D_2O, 25 °C) δ 8.21 (d, J = 6.3 Hz, 2H), 7.70 (d, J = 6.1 Hz, 2H), 7.63-7.57 (q, J = 7.8 Hz, 6H), 7.48-7.40 (m, 4H), 6.97 (d, J = 16.2 Hz, 1H), 3.94 (s, 3H). ^{13}C NMR (100 MHz, D_2O, 25 °C) δ 152.81, 143.69, 140.76, 139.51, 138.45, 134.13, 129.08, 128.80, 128.09, 126.72, 126.19, 123.48, 122.00, 46.51. HRMS (ESI) for $C_{20}H_{18}NCl$: calcd. $[M\text{-}Cl]^+$: 272.1439, found: 272.1436. Melting point: 209 °C.

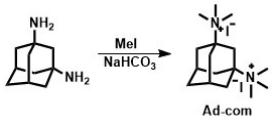

Scheme S3. The route of synthesis of Ad-com.

Synthesis of **Ad-com**[S2]

1,3-Adamantanediamine (50 mg, 0.3 mmol), MeI (0.19 mL,3 mmol) and $NaHCO_3$ (252 mg, 3 mmol) were dissolved in 10 ml acetonitrile, and then the reaction was heated at reflux for 72 h. The reaction mixture was filtered and concentrated solution by rotary evaporation. The

obtained curde product was recrystallizated in water (121 mg, 80%). ^{1}H NMR (400 MHz, D_2O, 25 °C) δ 3.15 (s, 18H), 2.74 (s, 2H), 2.36 (s, 2H), 2.17 (s, 8H), 1.68 (s, 2H). ^{13}C NMR (100 MHz, D_2O, 25 °C) δ 73.90, 48.99, 32.52, 32.12, 30.17. HRMS (ESI) for $C_{16}H_{32}N_2I_2$: calcd. $[M\text{-}I]^+$: 379.1610, found: 379.1608.

3、Characterization of TPA-SP and M-SP.

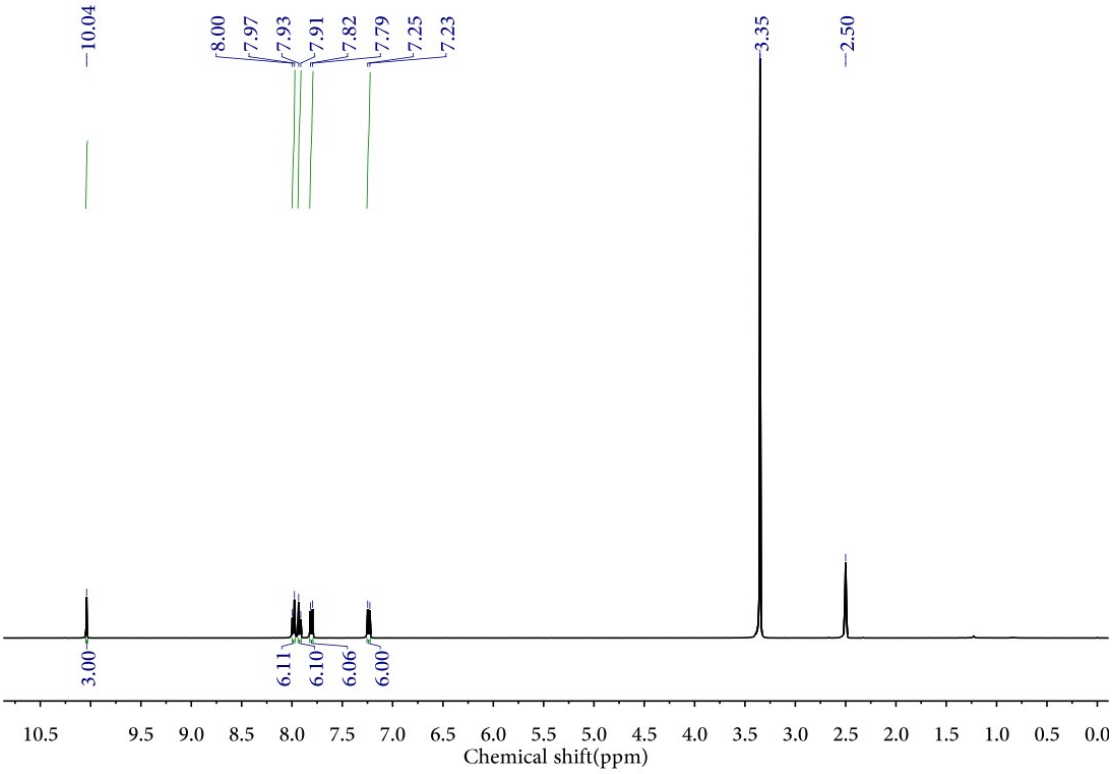

Figure S1. ^{1}H NMR spectrum (400 MHz, d_6-DMSO, 25 °C) of 3.

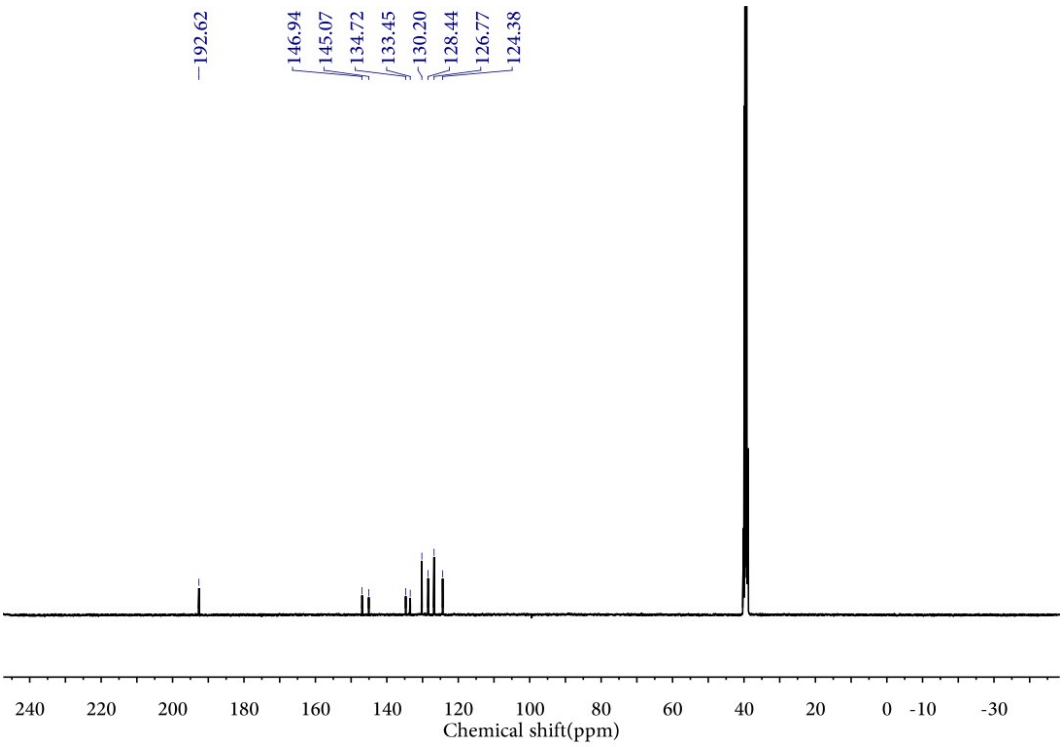

Figure S2. ^{13}C NMR spectrum (100 MHz, d_6-DMSO, 25 °C) of 3.

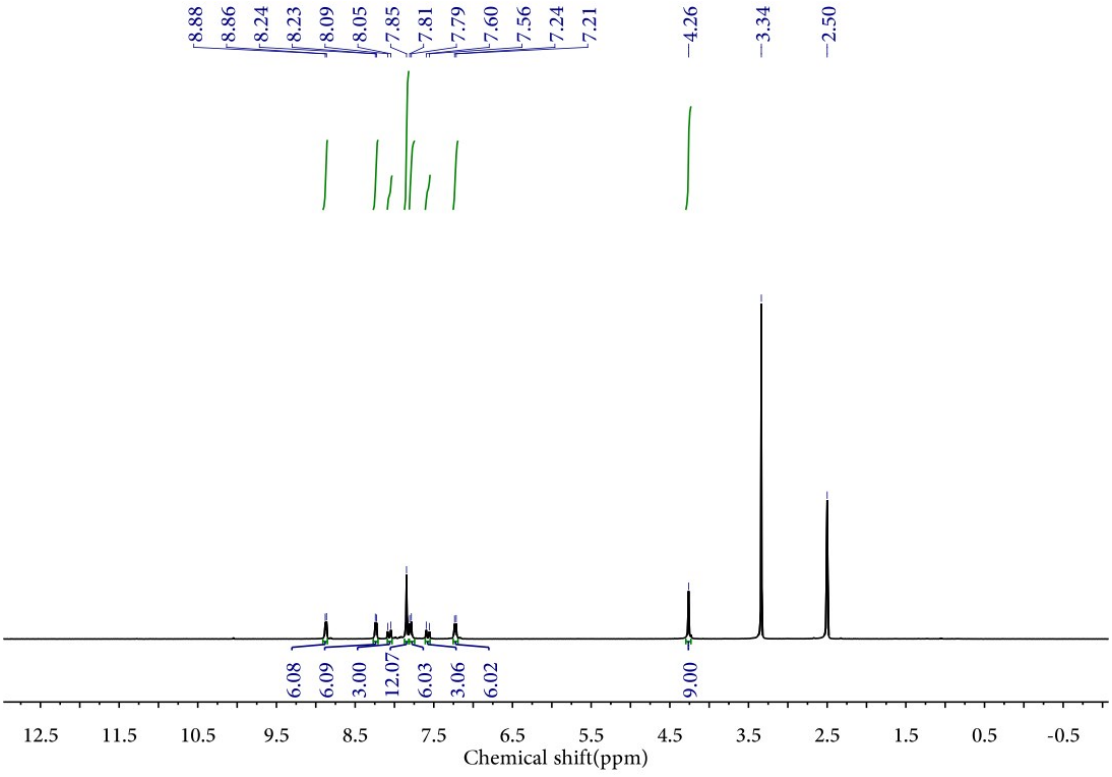

Figure S3. ^{1}H NMR spectrum (400 MHz, d_6-DMSO, 25 °C) of TPA-SP.

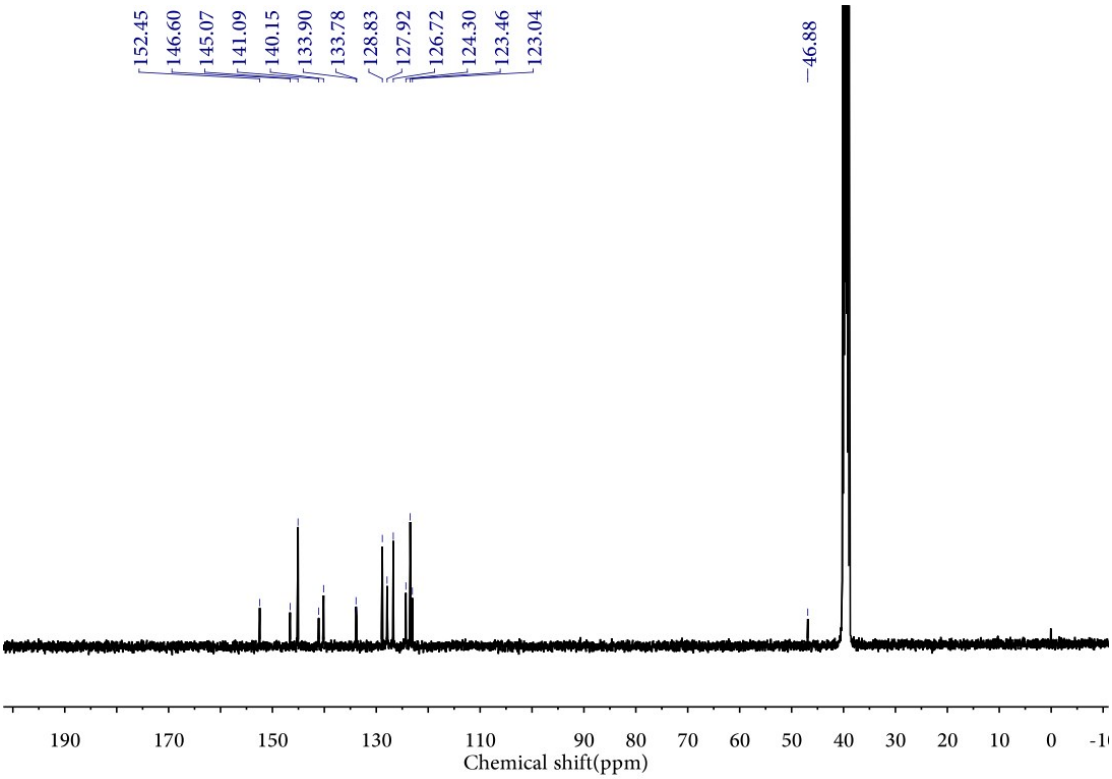

Figure S4. ^{13}C NMR spectrum (100 MHz, d_6-DMSO, 25 °C) of TPA-SP.

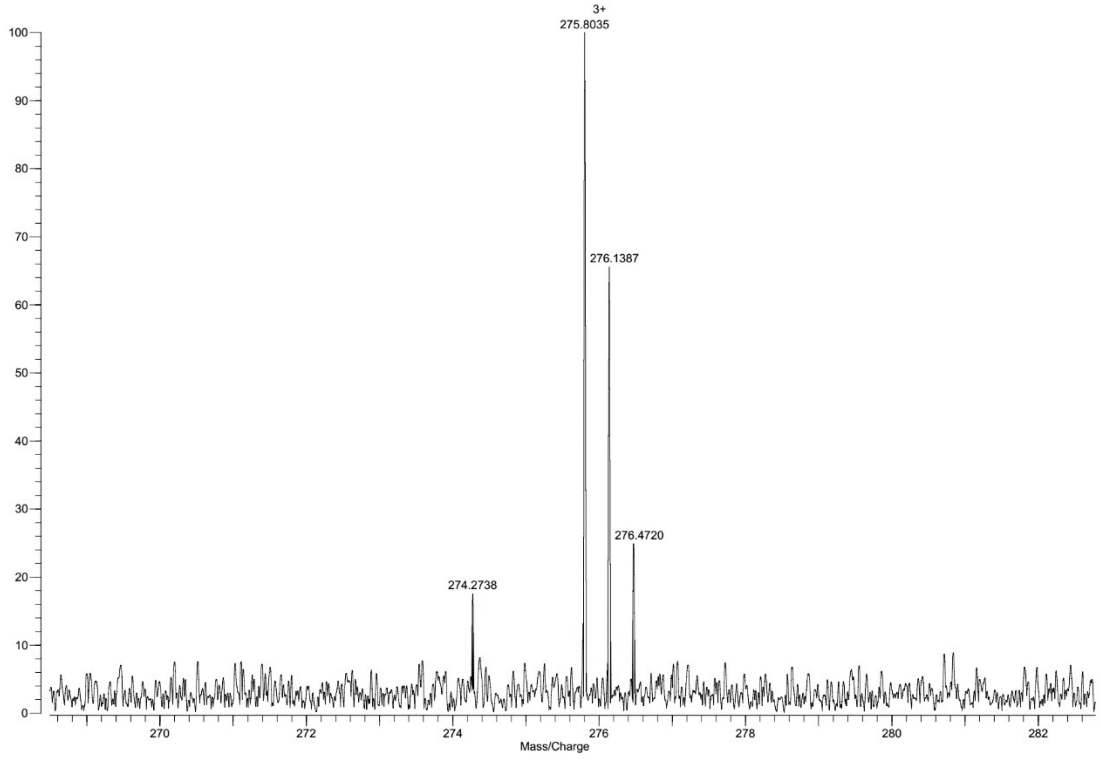

Figure S5. HRMS spectrum of TPA-SP ($C_{60}H_{51}N_4Cl_3$). The peak at *m/z* 275.8035 is assigned to $[M-3Cl]^+/3$, calcd.: 275.8038.

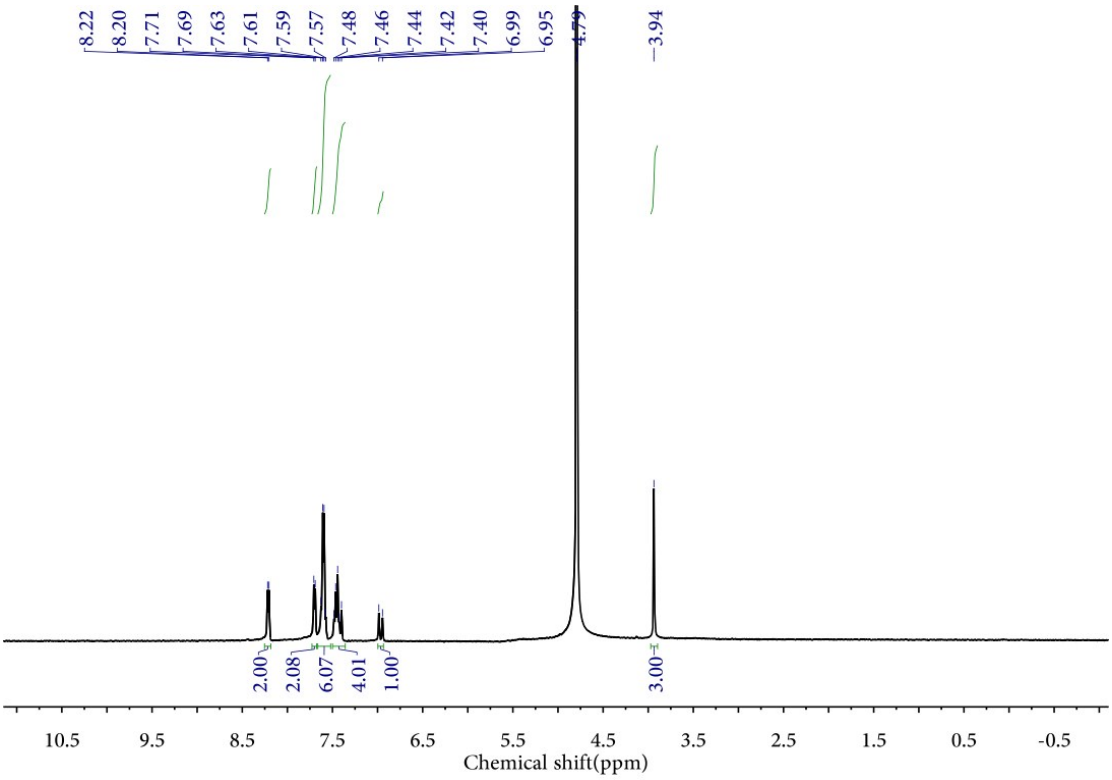

Figure S6. ^{1}H NMR spectrum (400 MHz, D_2O, 25 °C) of M-SP.

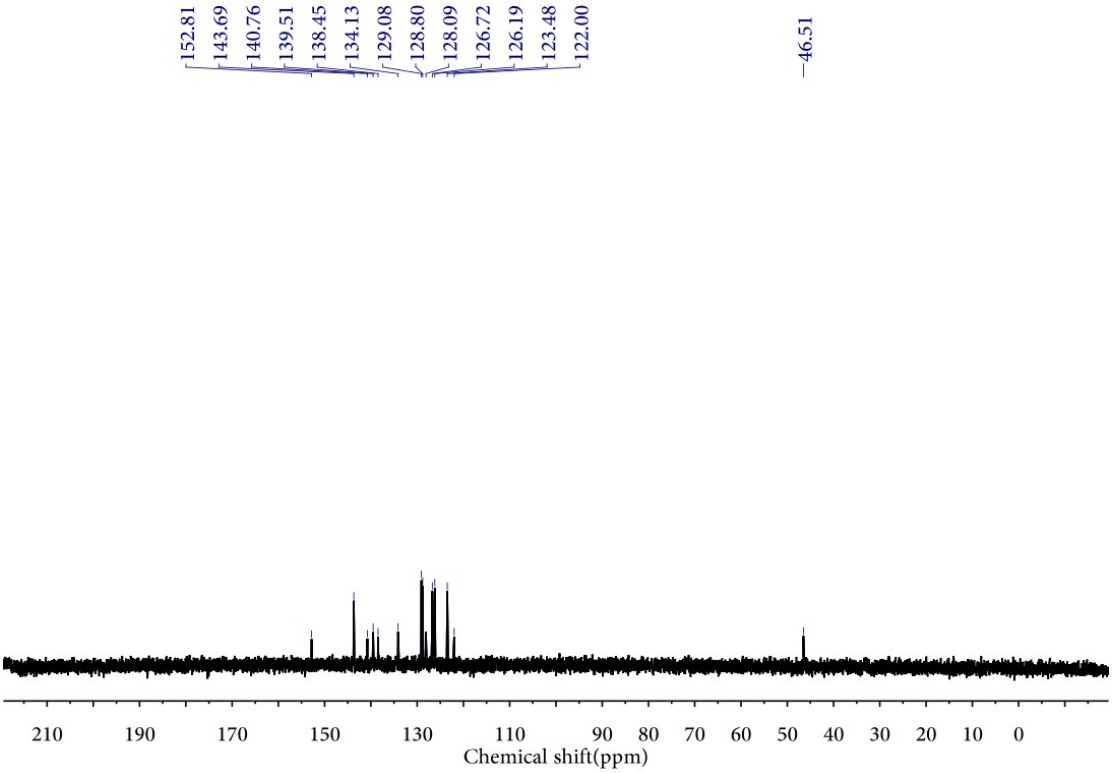

Figure S7. ^{13}C NMR spectrum (100 MHz, D_2O, 25 °C) of M-SP.

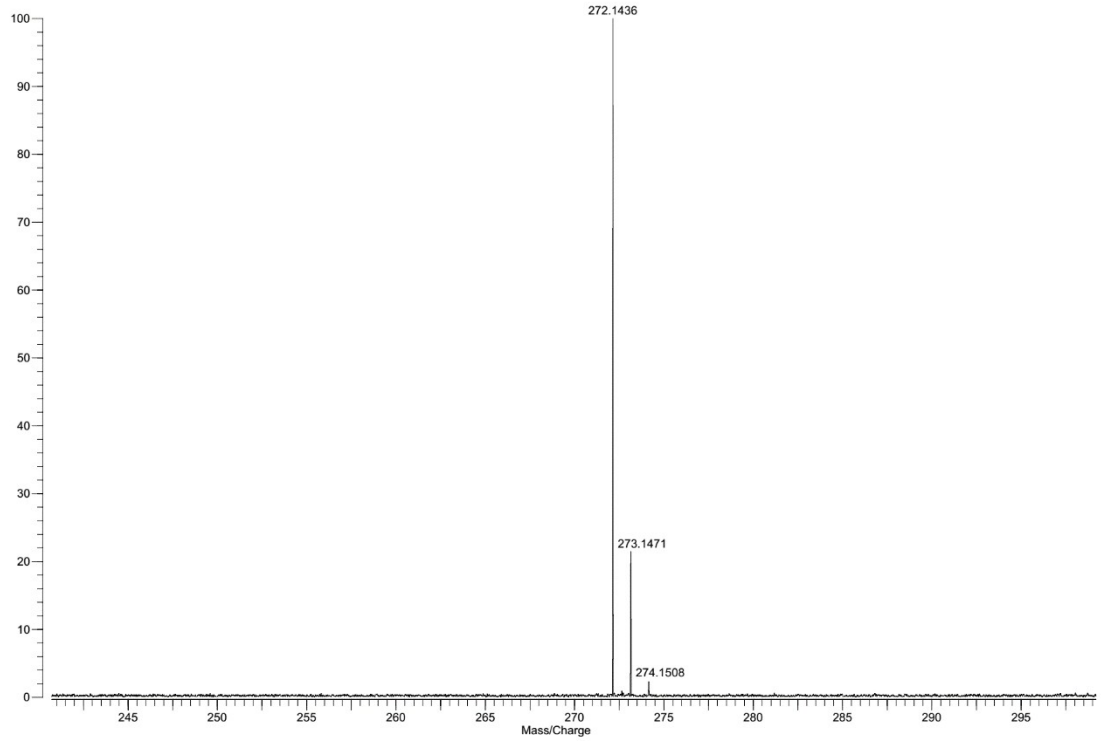

Figure S8. HRMS spectrum of M-SP ($C_{20}H_{18}NCl$). The peak at *m/z* 272.1436 is assigned to $[M\text{-}Cl]^+$, calcd.: 272.1439.

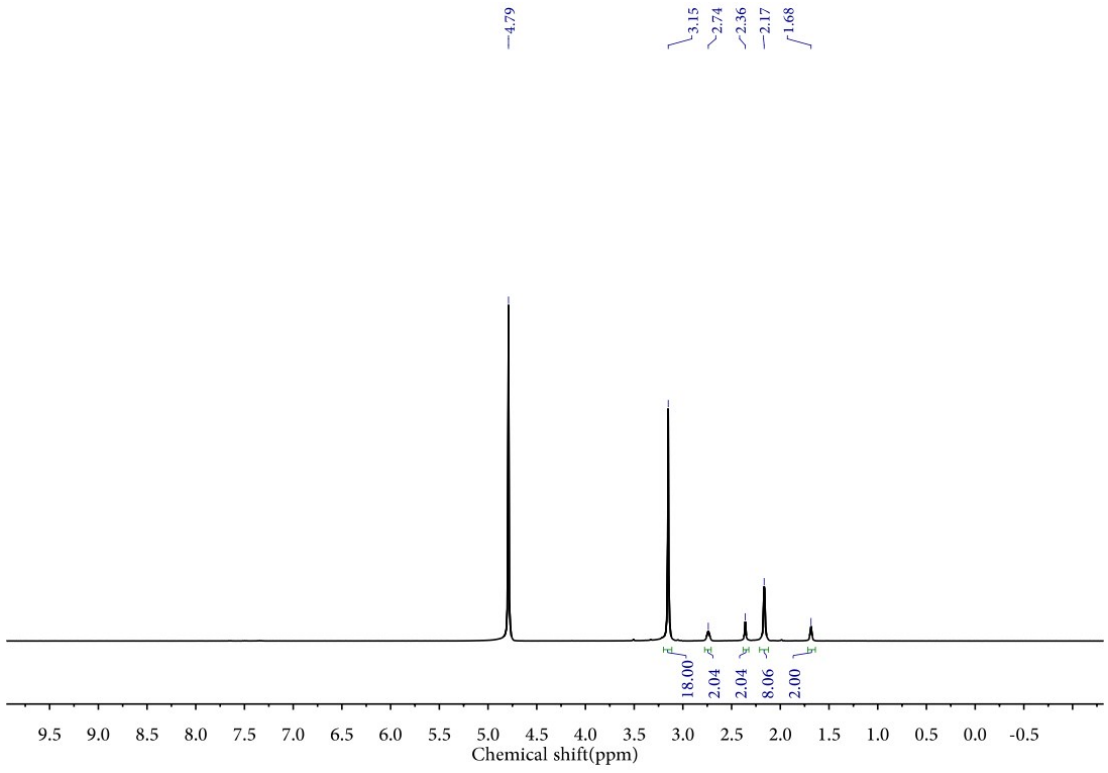

Figure S9. ^1H NMR spectrum (400 MHz, D_2O, 25 °C) of Ad-com.

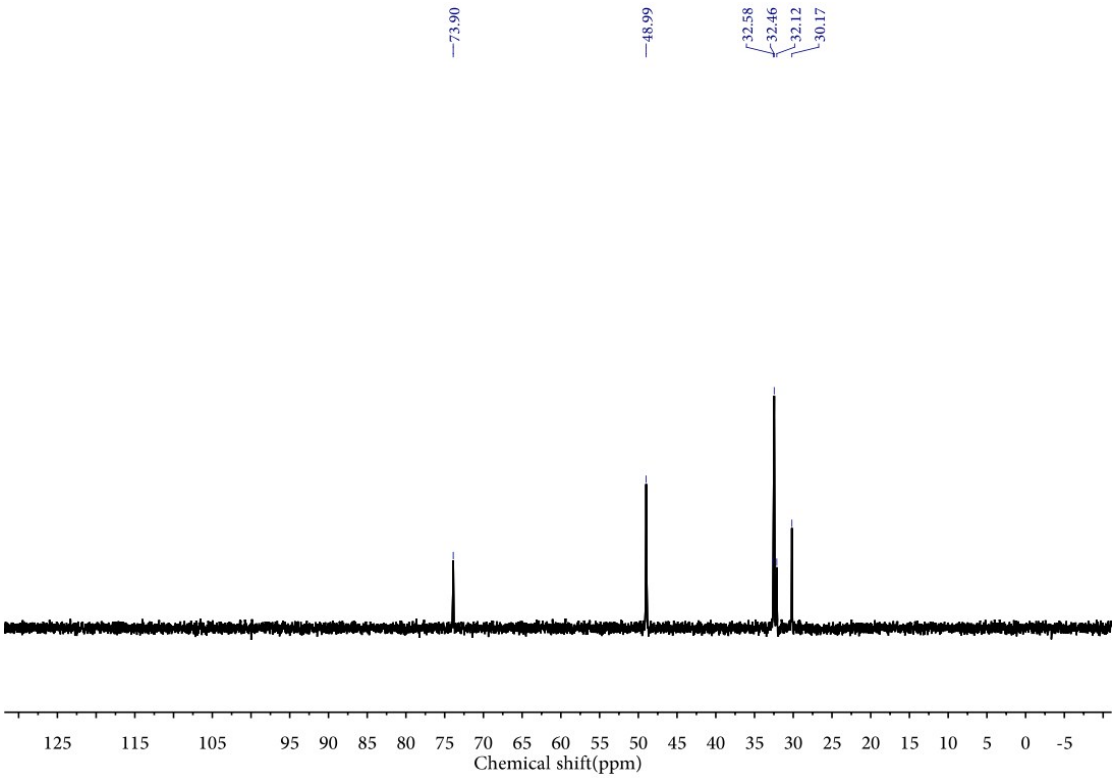

Figure S10. ^{13}C NMR spectrum (100 MHz, D_2O, 25 °C) of Ad-com.

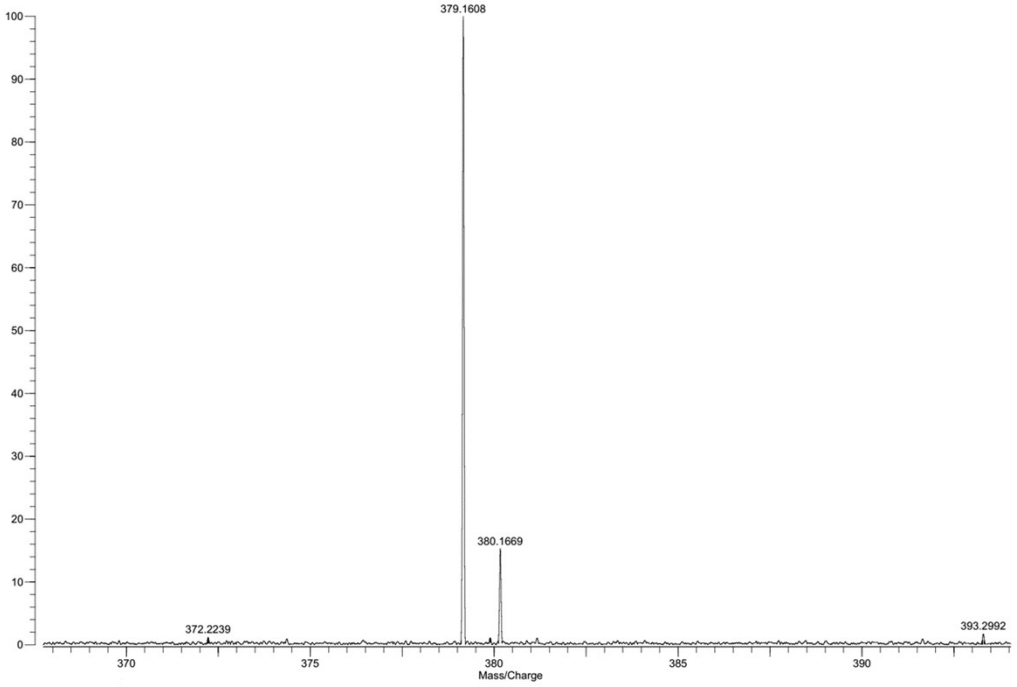

Figure S11. HRMS spectrum of Ad-com ($C_{16}H_{32}N_2I_2$). The peak at *m/z* 379.1608 is assigned to $[M\text{-}I]^+$, calcd.: 379.1610.

4、Characterization of TPA-SP⊂CB[8] complex.

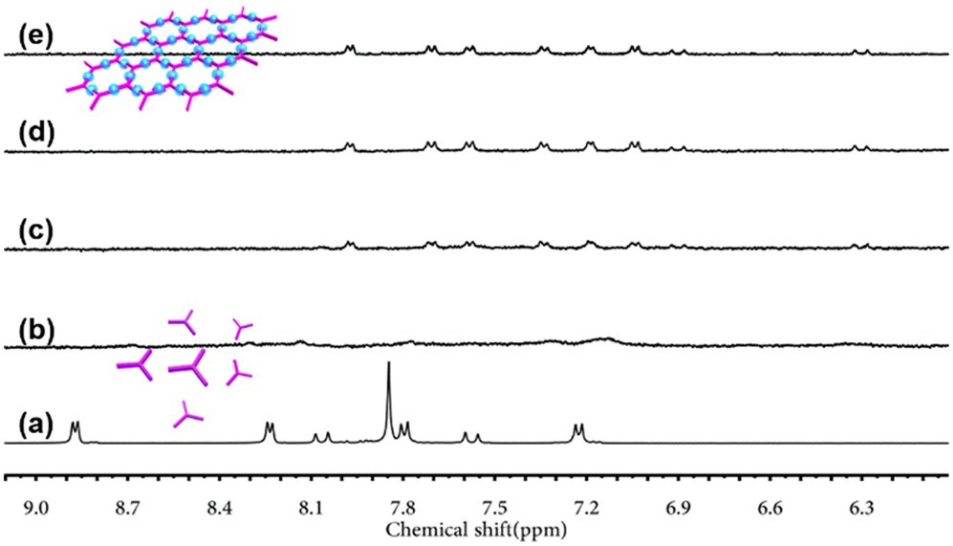

Figure S12. Partial ^{1}H NMR spectra (400 MHz, D_2O, 25 °C) of (a) free TPA-SP in d_6-DMSO (1.0 mM), (b)-(e) different ratio of TPA-SP:CB[8] in D_2O ([TPA-SP] = 0.2 mM), (b) free TPA-SP, (c) TPA-SP:CB[8] = 1:1, (d) TPA-SP:CB[8] = 1:1.5, (e) TPA-SP:CB[8] = 1:2.

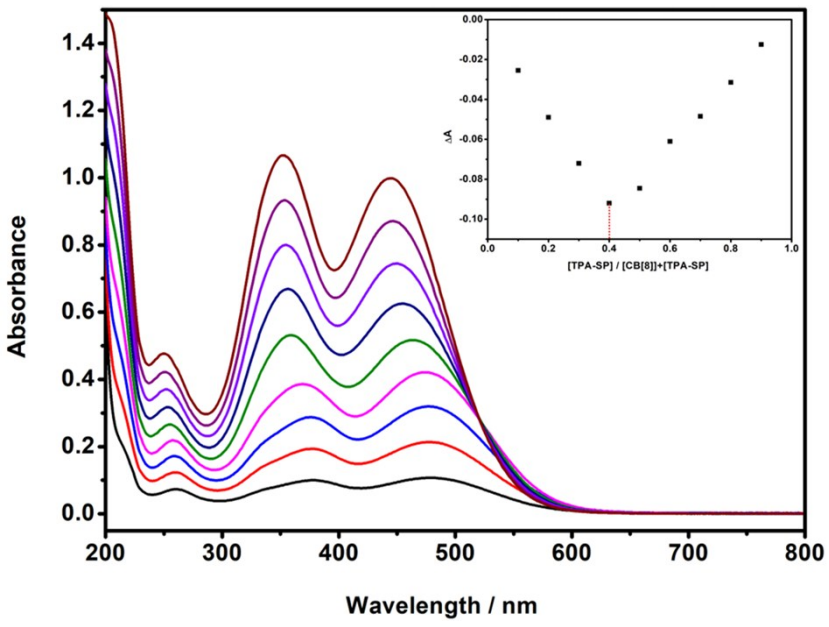

Figure S13. UV-vis spectra of TPA-SP⊂CB[8] complex ([TPA-SP] + [CB[8]] = 0.02 mM) at different ratio in aqueous solution, measured in a 10 mm quartz cell. Inset: Job's plot showing

the 2:3 stoichiometry of the complex between TPA-SP and CB[8], where ΔA means the absorbance difference value with free TPA-SP under the same concentration at 443 nm.

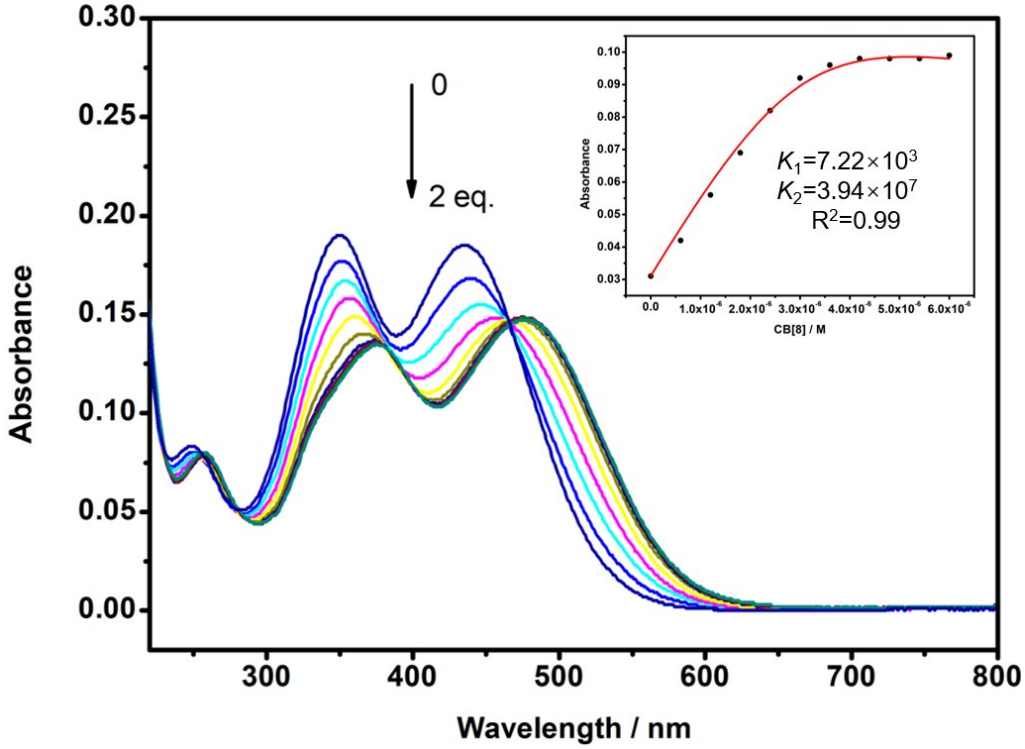

Figure S14. UV/vis spectral changes of TPA-SP upon addition of CB[8] in water ([TPA-SP] = 3 × 10^{-6} M, [CB[8]] = 0, 0.6, 1.2, 1.8, 2.4, 3.0, 3.6, 4.2, 4.8, 5.4 and 6.0 × 10^{-6} M, respectively). Inset: The nonlinear least-squares analysis of absorbance change at 523 nm to calculate the K_a value for TPA-SP⊂CB[8] complex. This result indicates that the inclusion complexation of first SP unit in the cavity of CB[8] was be beneficial to the capture of second one, thus facilitating the eventual formation of stable 2D supramolecular assembly.[S3]

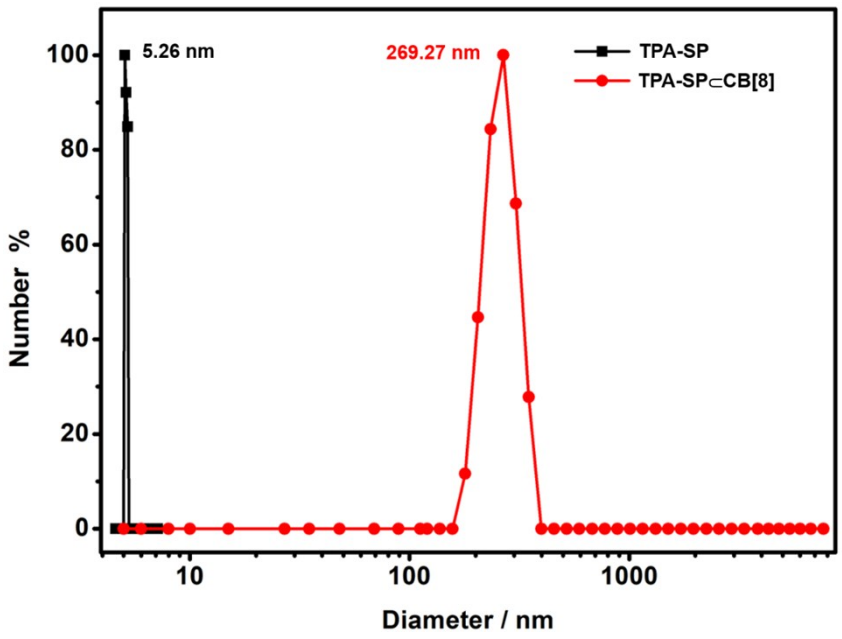

Figure S15. DLS profiles of free TPA-SP (black line) and TPA-SP⊂CB[8] (red line) in water ([TPA-SP] = 0.2 mM).

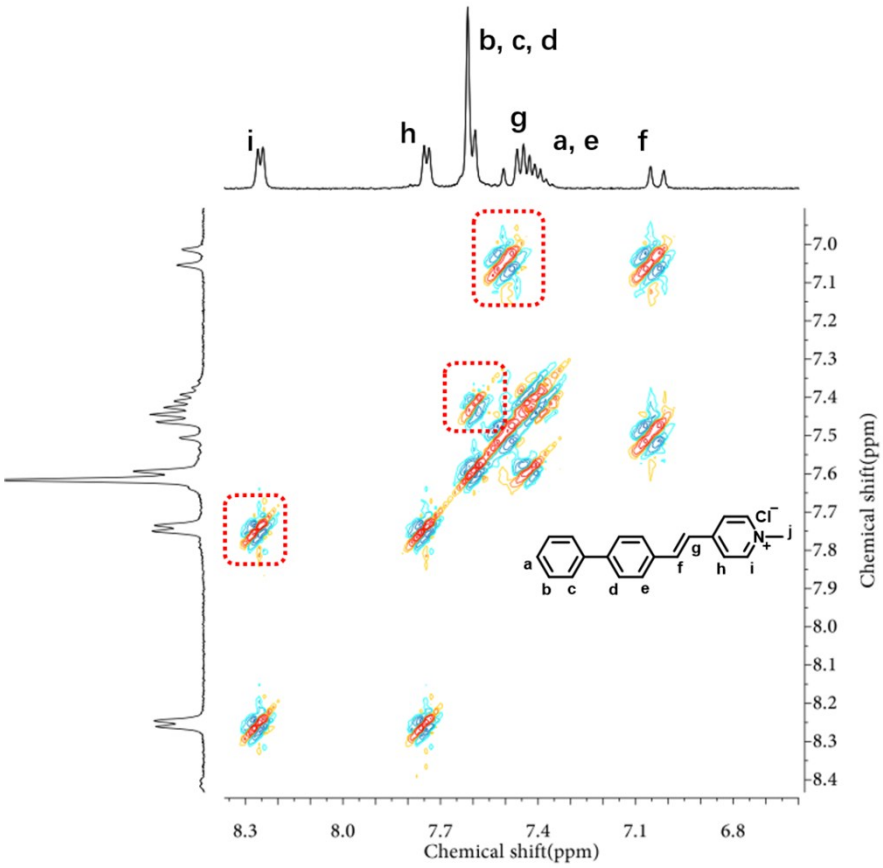

Figure S16. ^{1}H-^{1}H COSY spectrum (400 MHz, D_2O, 25 °C) of M-SP.

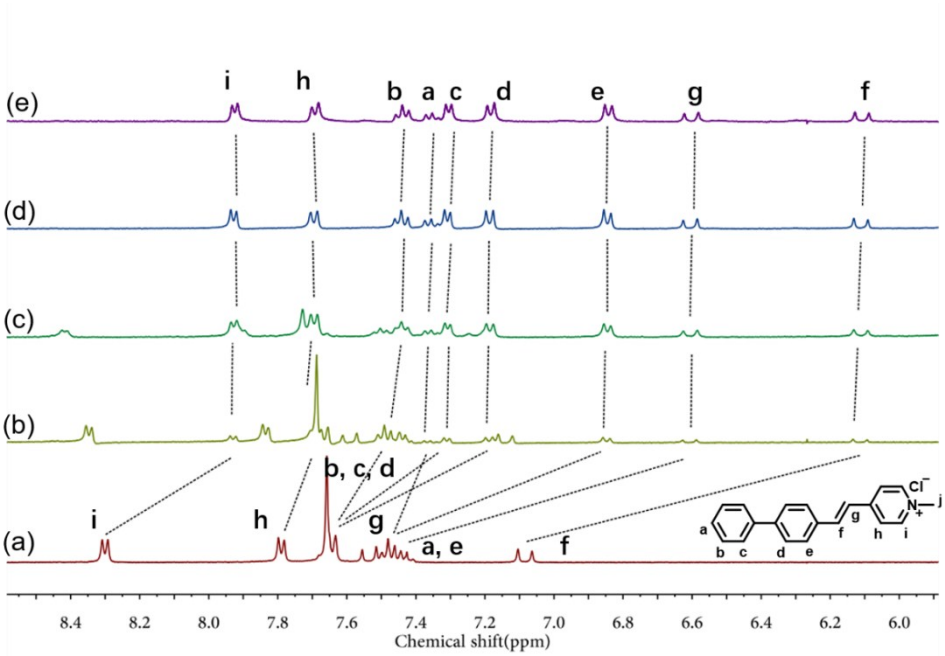

Figure S17. Partial ^{1}H NMR spectra (400 MHz, D_2O, 25 ℃) of (a) free M-SP, (b) M-SP:CB[8] = 1:0.1, (c) M-SP:CB[8] = 1:0.3, (d) M-SP:CB[8] = 1:0.5, (e) M-SP:CB[8] = 1:0.7 ([M-SP] = 2 mM).

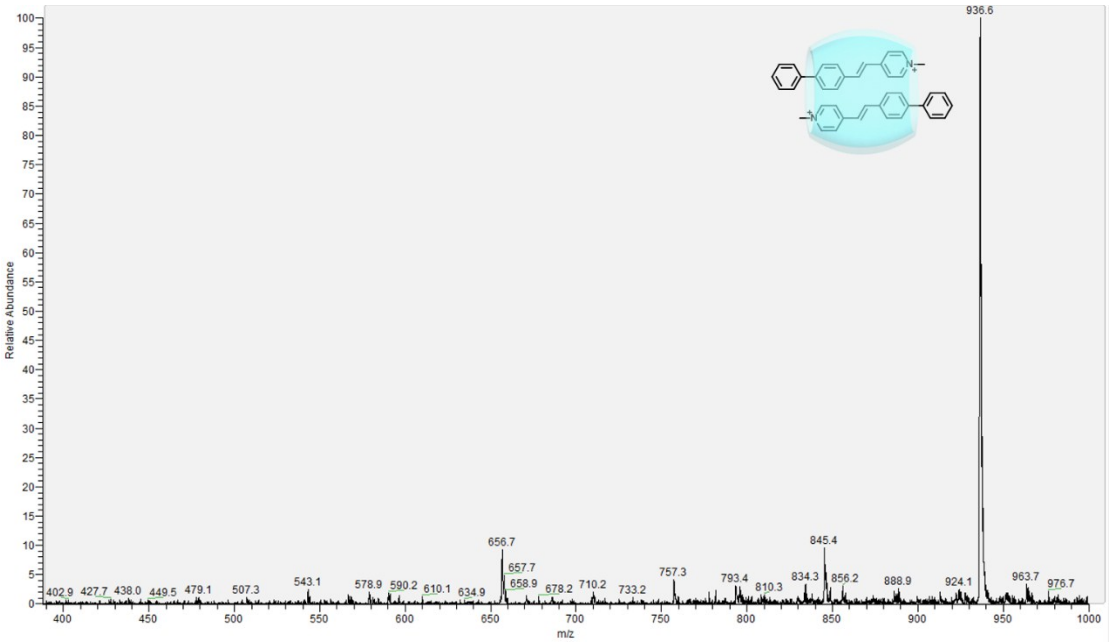

Figure S18. MS spectrum of M-SP⊂CB[8] ($C_{88}H_{84}N_{34}O_{16}Cl_2$). The peak at *m/z* 936.6 is assigned to $[M-2Cl]^{+}/2$, calcd.: 936.3.

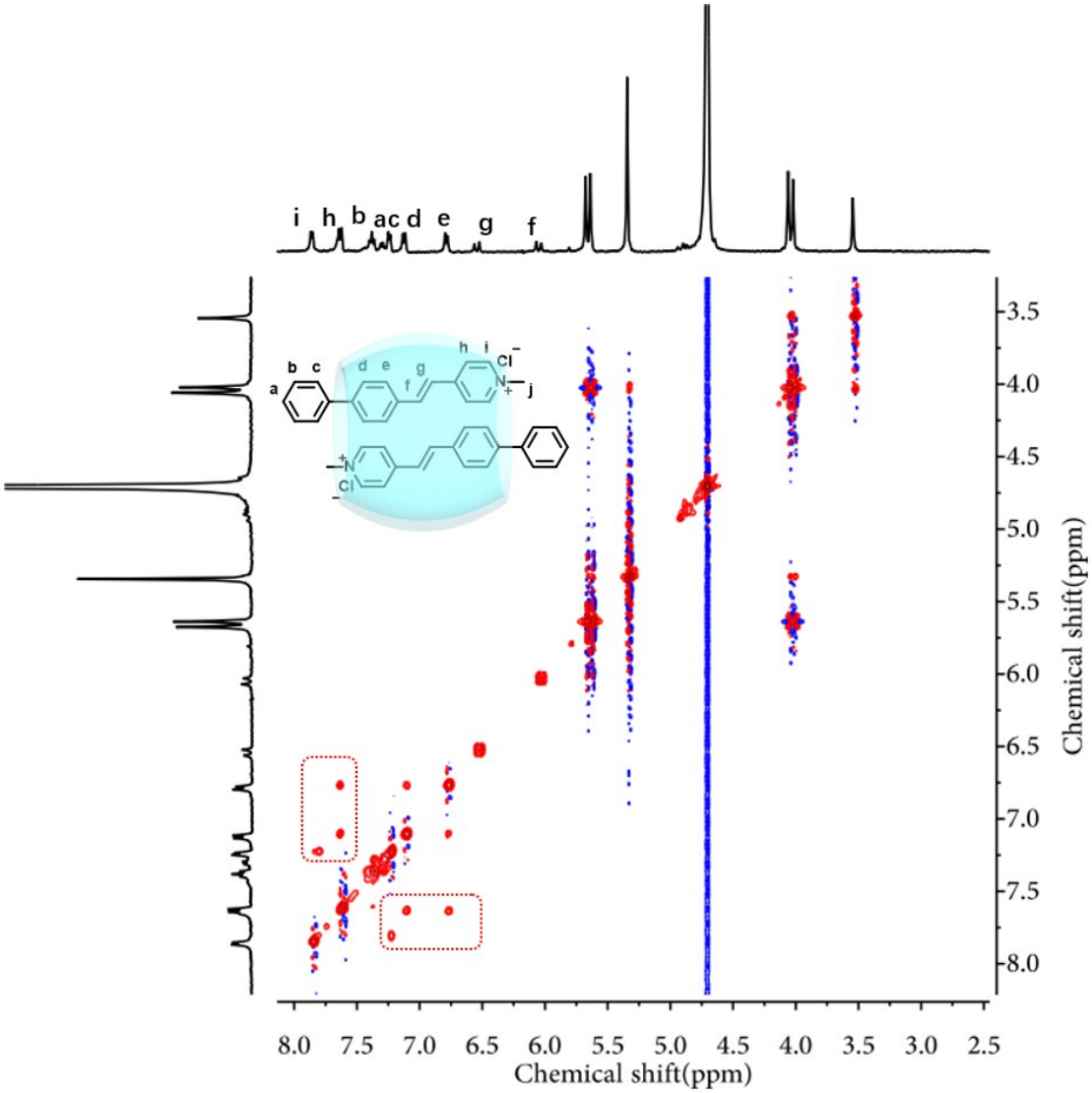

Figure S19. 2D NOESY spectrum (400 MHz, D_2O, 25 °C) of M-SP:CB[8] = 1:0.5 ([M-SP] = 2 mM).

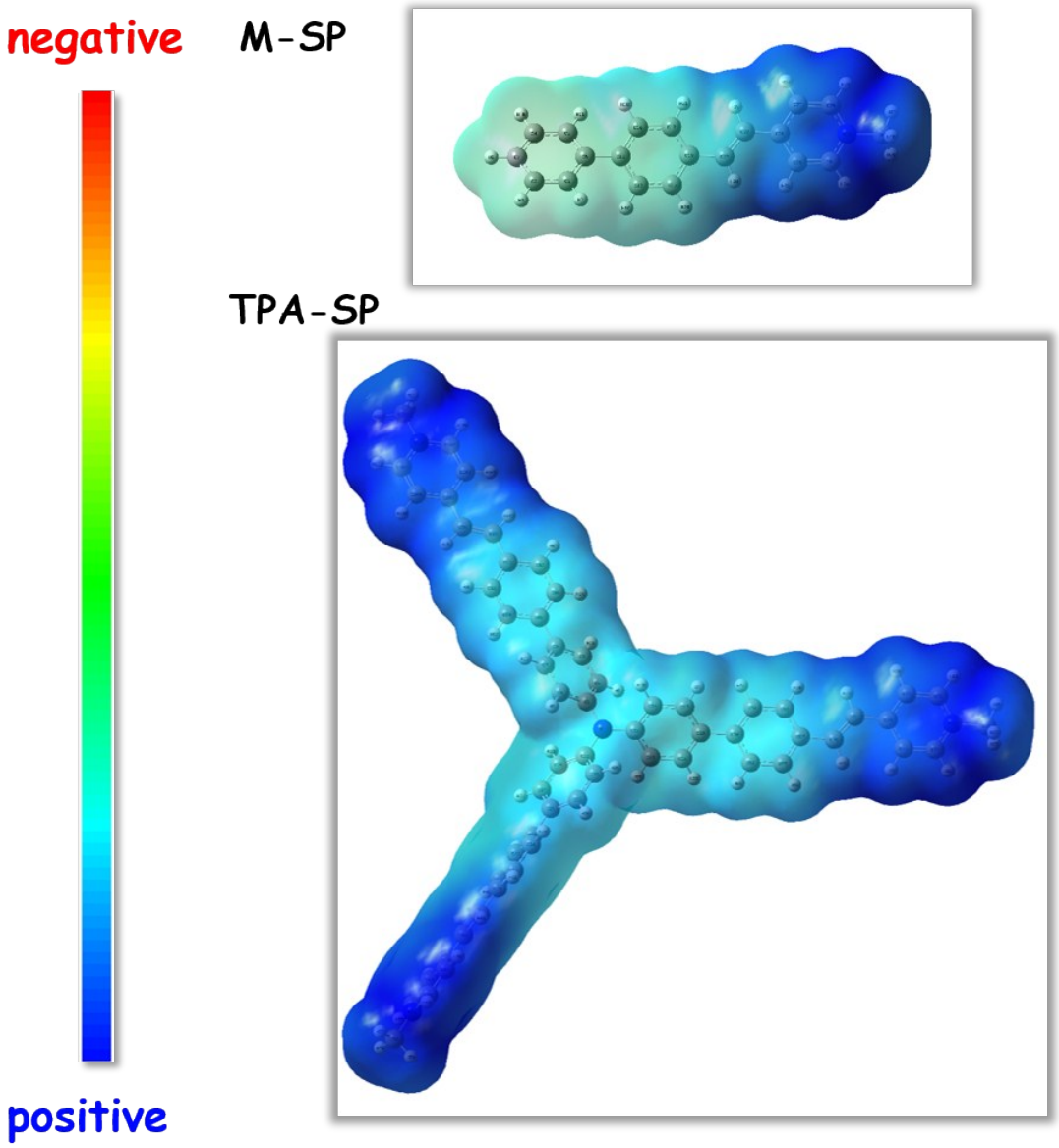

Figure. 20 Electrostatic potential surfaces of M-SP and TPA-SP. Blue and red represent positive and negative electrostatic potentials, respectively.

DFT calculations were performed at B3LYP/6-31G(d,p)//SMD_{water} level using Gaussian16. From geometry optimization and electrostatic potential analysis of TPA-SP and M-SP, we found that the electrostatic potential distribution at their site of inclusion is very similar. Hence, we think TPA-SP and M-SP are possible to have the same stacking pattern included in CB[8].

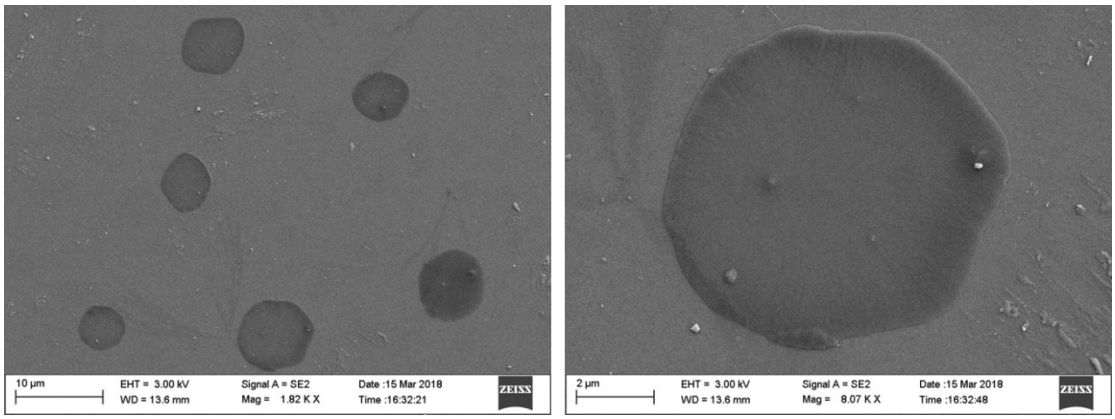

Figure S21. SEM images of TPA-SP⊂CB[8].

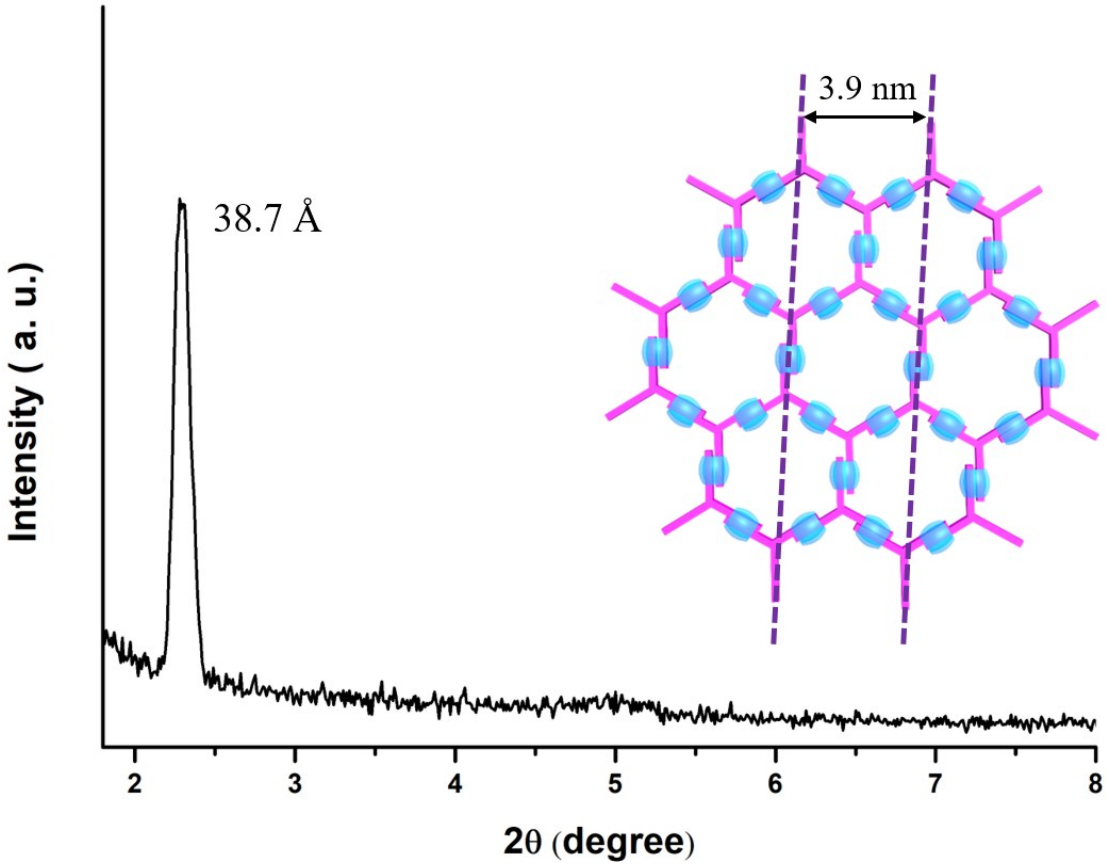

Figure S22. Grazing incidence X-ray diffraction (GI-SAXS) of TPA-SP⊂CB[8] in solid form.

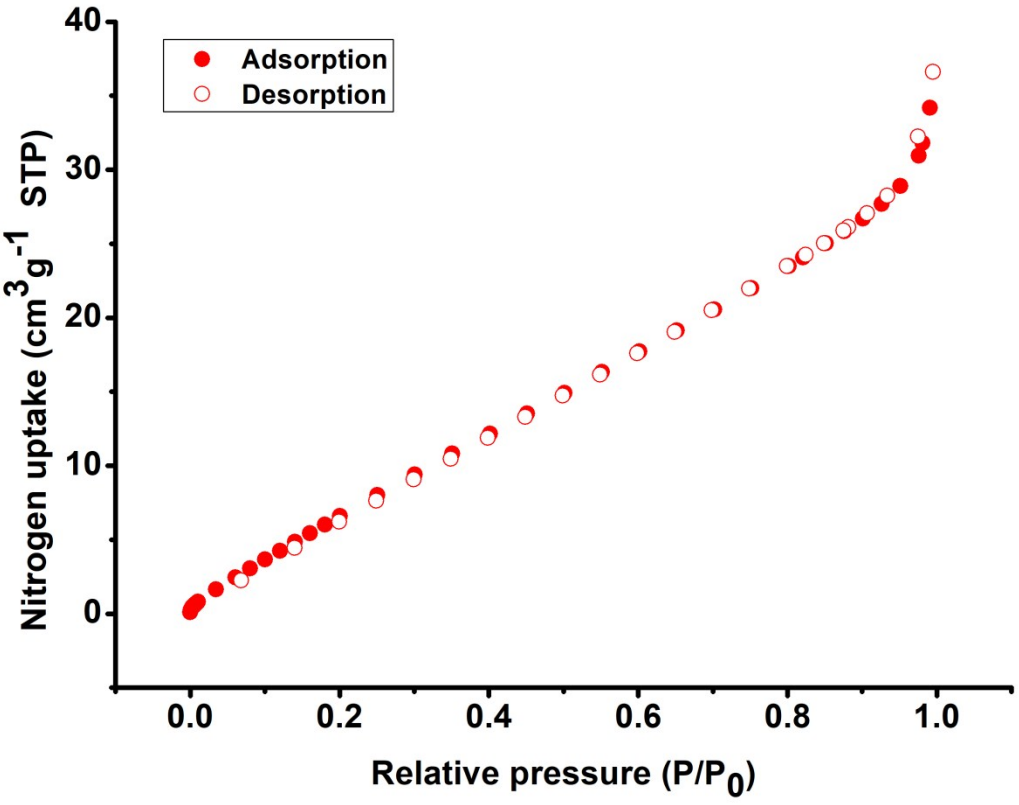

Figure S23. N_2 gas adsorption analysis of TPA-SP⊂CB[8].

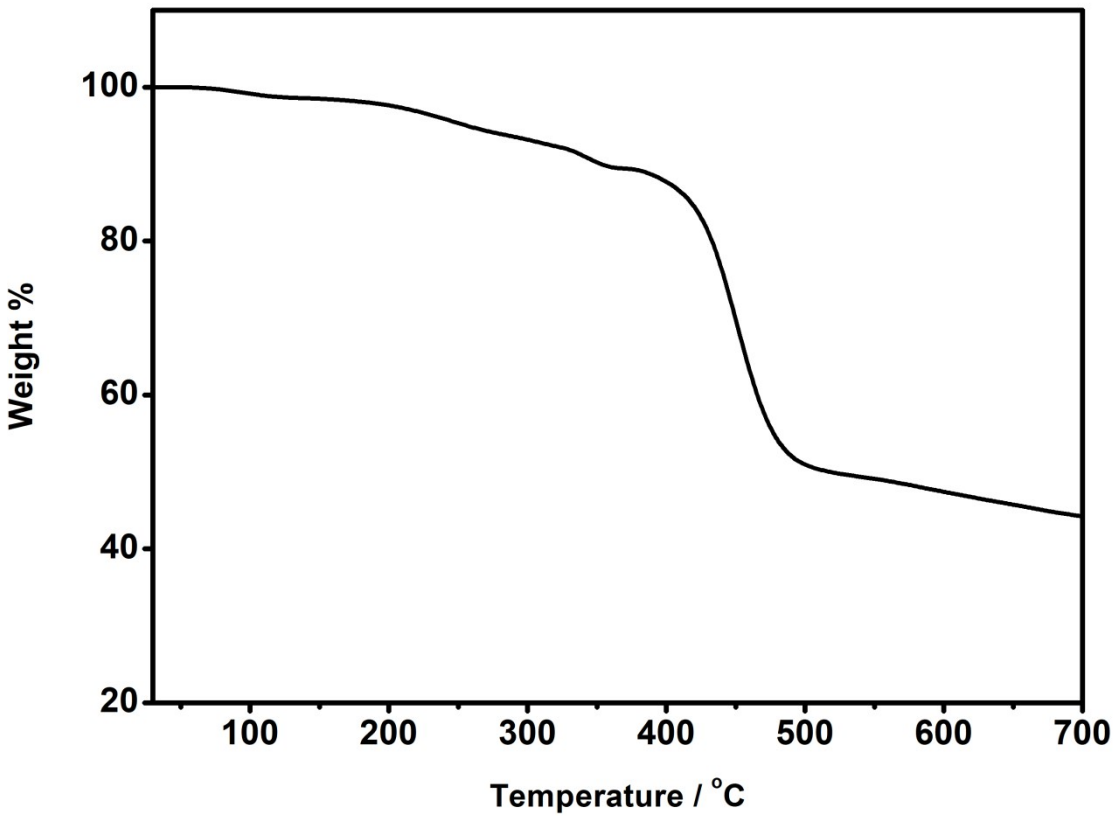

Figure S24. TGA of TPA-SP⊂CB[8].

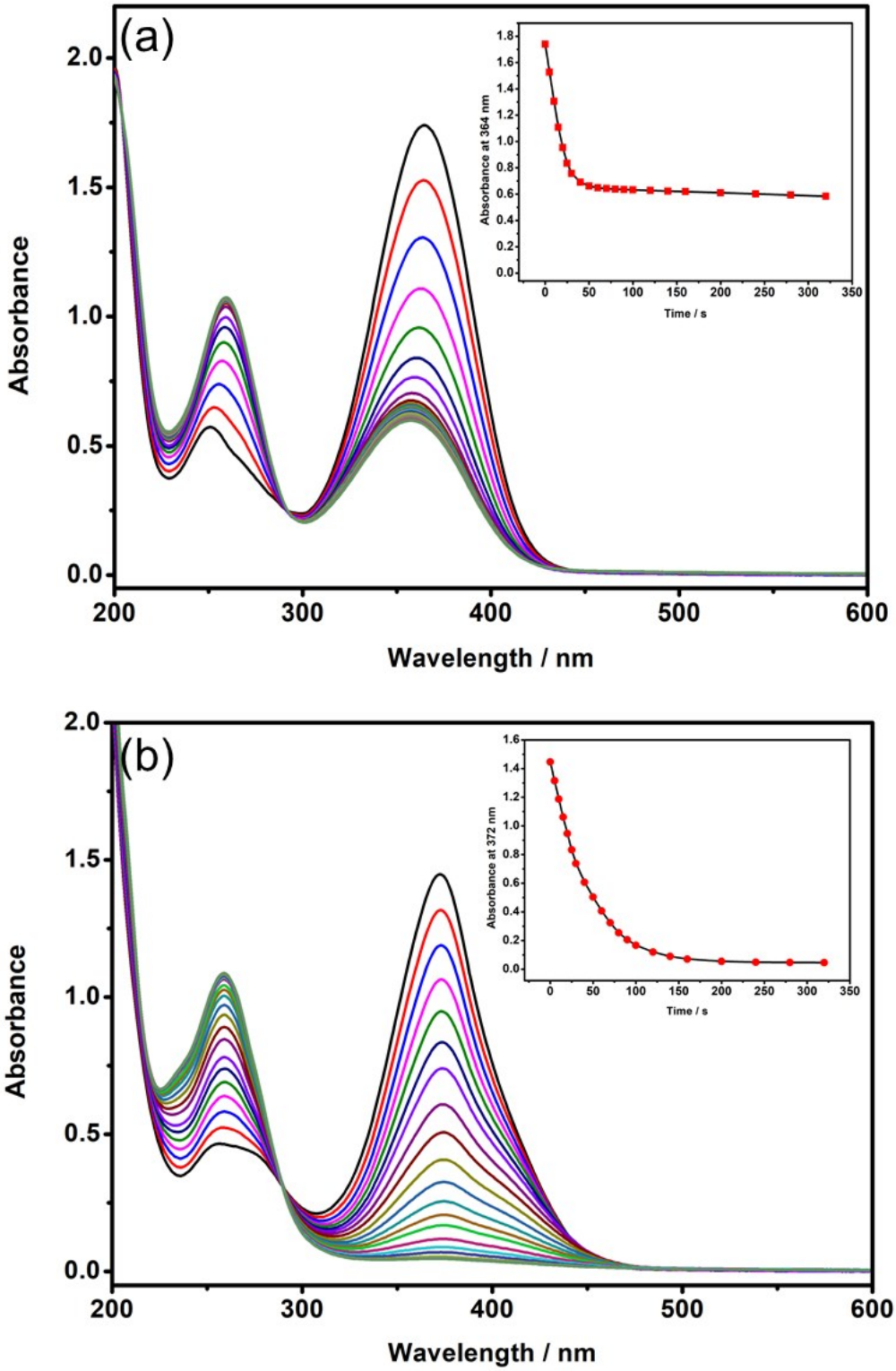

Figure S25. UV-vis absorbance change of (a) free M-SP, (b) M-SP:CB[8] = 1:0.5 under irradiation by 365 nm, the light path was 1 mm ([M-SP] = 0.4 mM, inset: absorbance changes versus irradiation time).

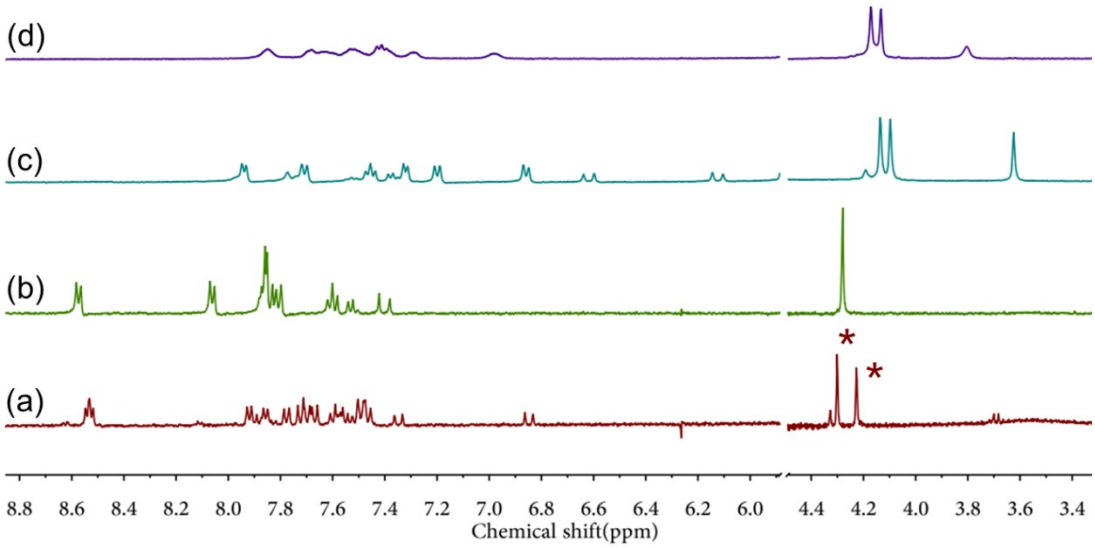

Figure S26. Partial ^{1}H NMR spectra (400 MHz, D_2O, 25 ℃) of (a) free M-SP after irradiation at 365 nm for 10 min, (b) free M-SP, (c) M-SP:CB[8] = 1:0.5, (d) M-SP:CB[8] = 1:0.5 after irradiation at 365 nm for 10 min ([M-SP] = 0.4 mM, the molar ratio of photoisomerization to photodimerization is calculated via integration of methyl unit, marked with '*' in (a)).

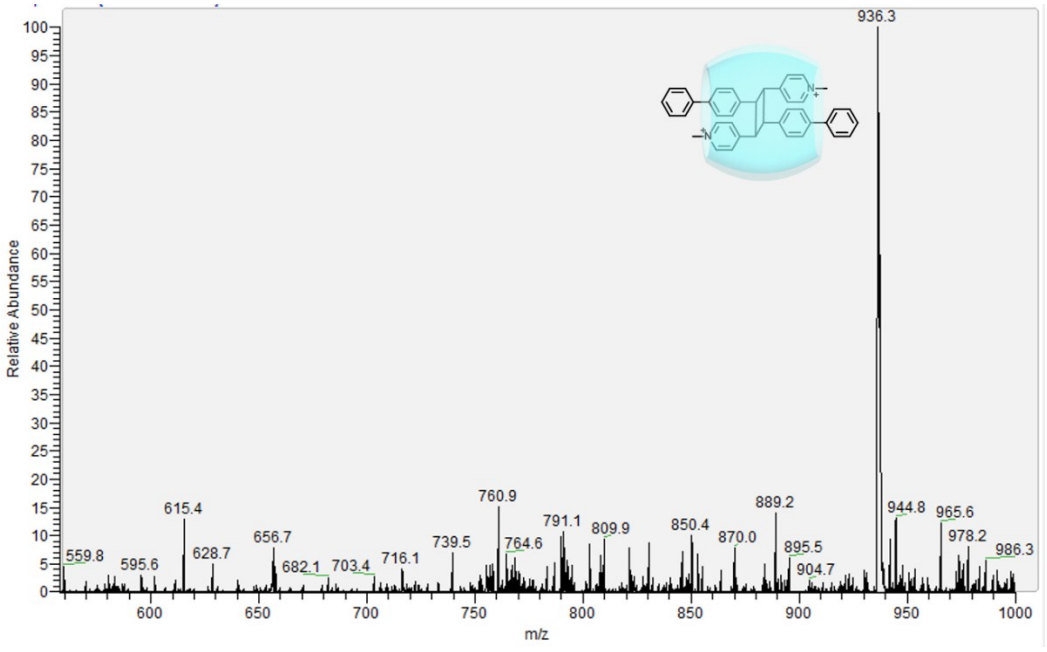

Figure S27. MS spectrum of M-SP⊂CB[8] after irradiation at 365 nm for 10 min ($C_{88}H_{84}N_{34}O_{16}Cl_2$). The peak at *m/z* 936.3 is assigned to $[M-2Cl]^{2+}/2$, calcd.: 936.3.

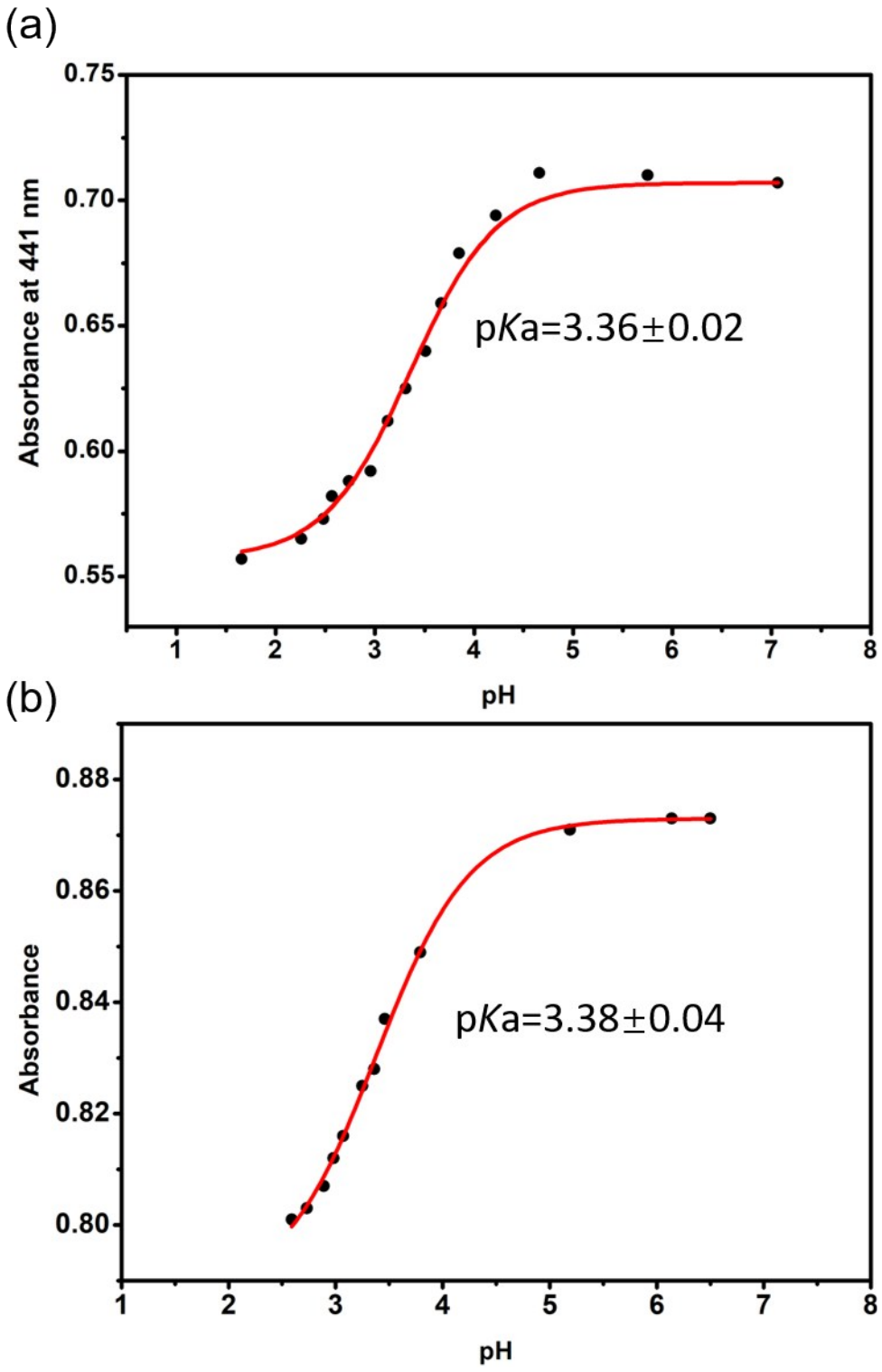

Figure S28. pK_a value of (a) free TPA-SP and (b) TPA-SP⊂CB[8].

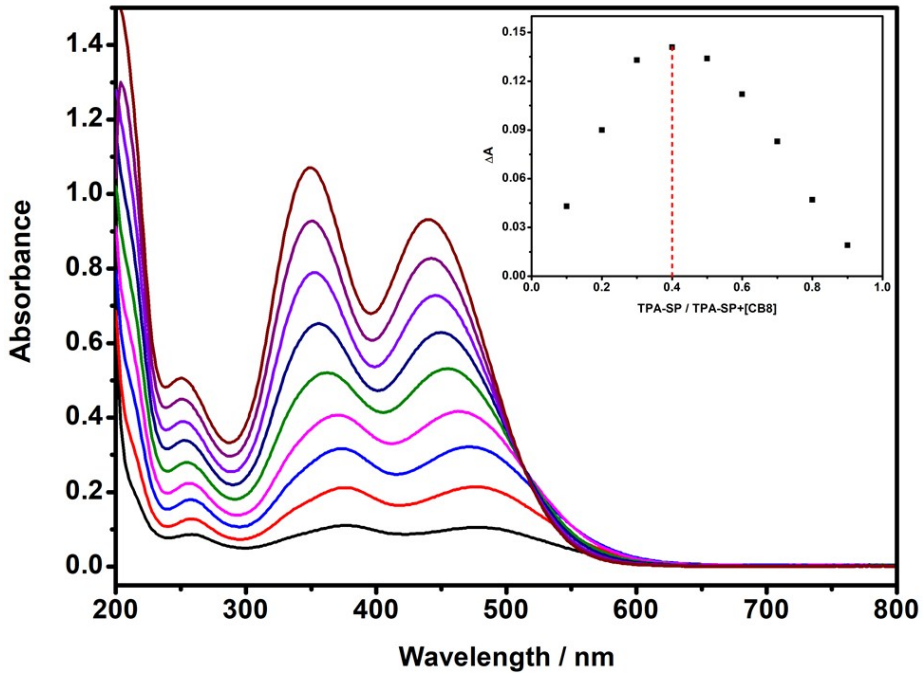

Figure S29. UV-vis spectra of TPA-SP⊂CB[8] complex ([TPA-SP] + [CB[8]] = 0.02 mM) at different ratio in 50 mM glycine-hydrochloric acid buffer (pH = 2.2), measured in a 10 mm quartz cell. Inset: Job's plot showing the 2:3 stoichiometry of the complex between TPA-SP and CB[8], where ΔA means the absorbance difference value with free TPA-SP under the same concentration at 485 nm.

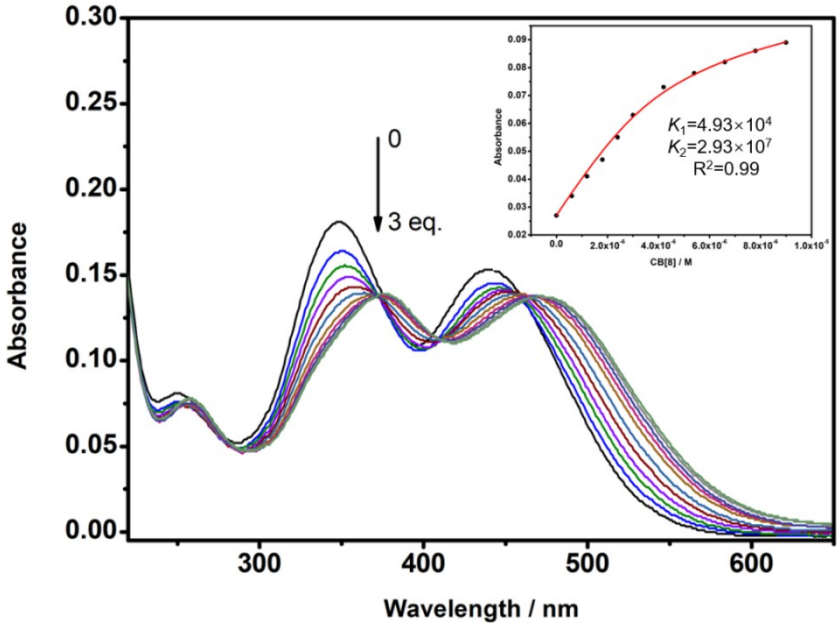

Figure S30. UV/vis spectral changes of TPA-SP upon addition of CB[8] in 50 mM glycine-hydrochloric acid buffer (pH = 2.2), ([TPA-SP] = 3 × 10^{-6} M, [CB[8]] = 0, 0.6, 1.2, 1.8, 2.4, 3.0, 4.2, 5.4, 6.6, 7.8, and 9.0 × 10^{-6} M, respectively). Inset: The nonlinear least-squares analysis of absorbance change at 523 nm to calculate the K_a value for TPA-SP⊂CB[8] complex.

5、Characterization of TPA-SP_{PD}⊂CB[8].

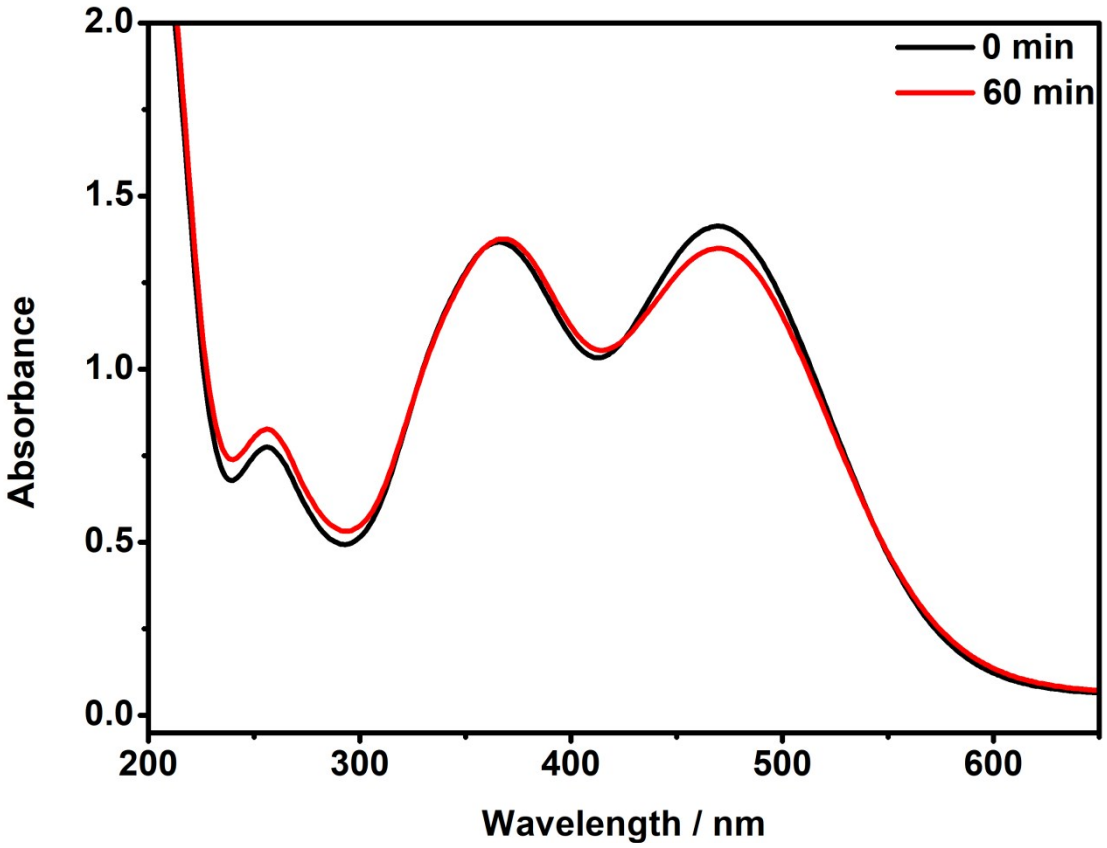

Figure S31. UV/vis spectra change of TPA-SP⊂CB[8] (as neutral state) under irradiation by 420 nm ([TPA-SP] = 0.2 mM, the light path is 1 mm).

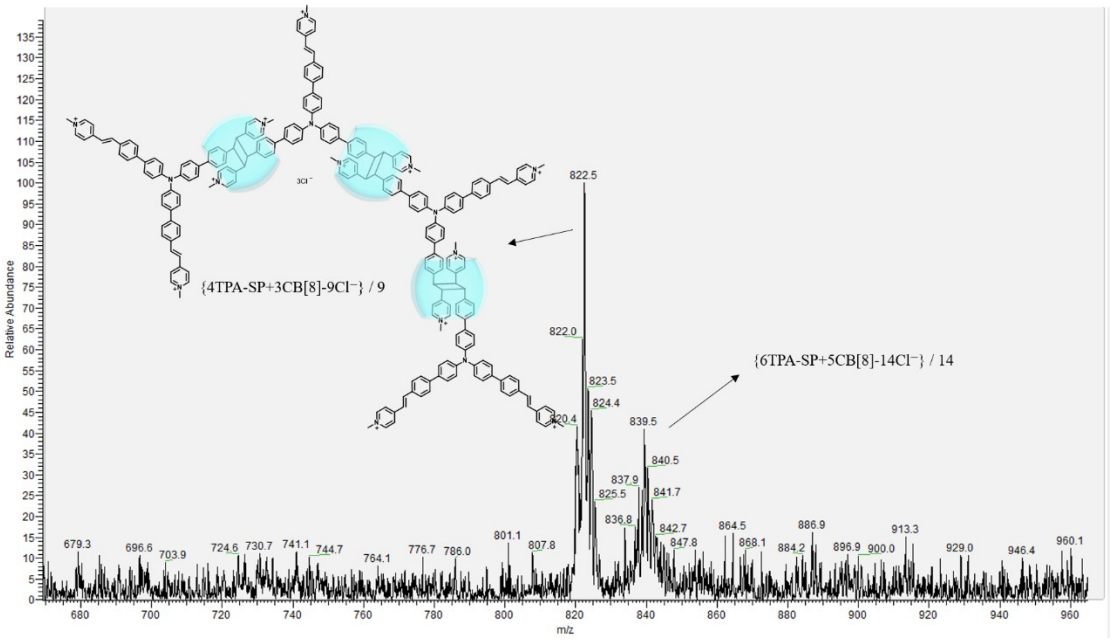

Figure S32. MS spectrum of TPA-SP⊂CB[8] after irradiation at 420 nm for 10 min. The peak at *m/z* 822.5 is assigned to $[C_{384}H_{348}O_{48}N_{112}Cl_{12}—9Cl]^{9+}/9$, calcd.: 822.9; The peak at *m/z* 839.5 is assigned to $[C_{600}H_{546}O_{80}N_{184}Cl_{18}—14Cl]^{14+}/14$, calcd.: 839.1.

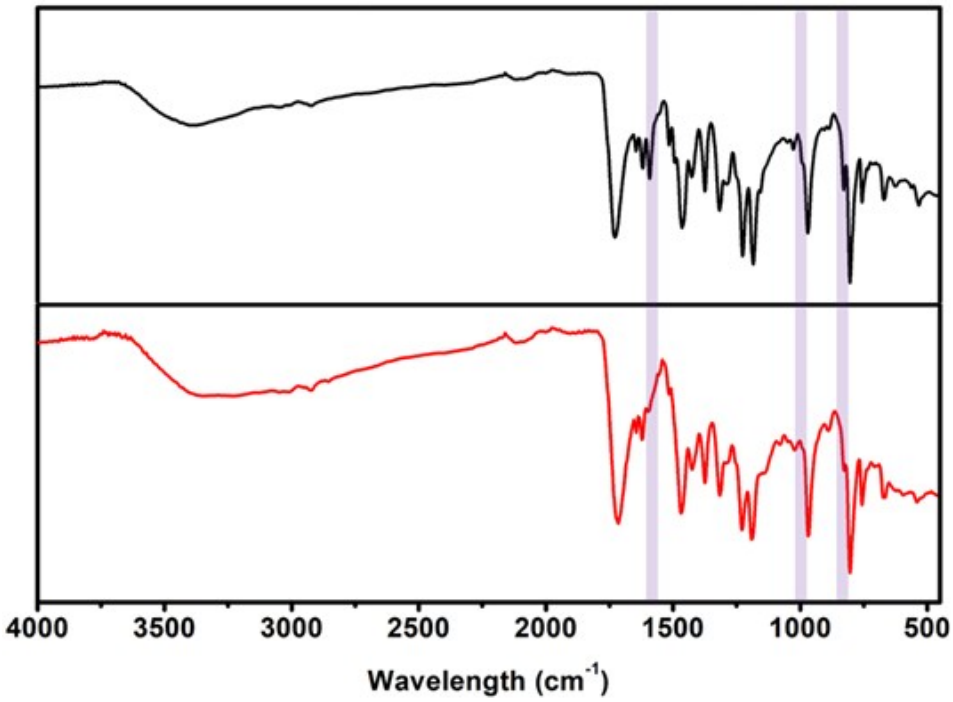

Figure S33. FTIR spectra of TPA-SP⊂CB[8] (black line) and TPA-SP_{PD}⊂CB[8] (red line).

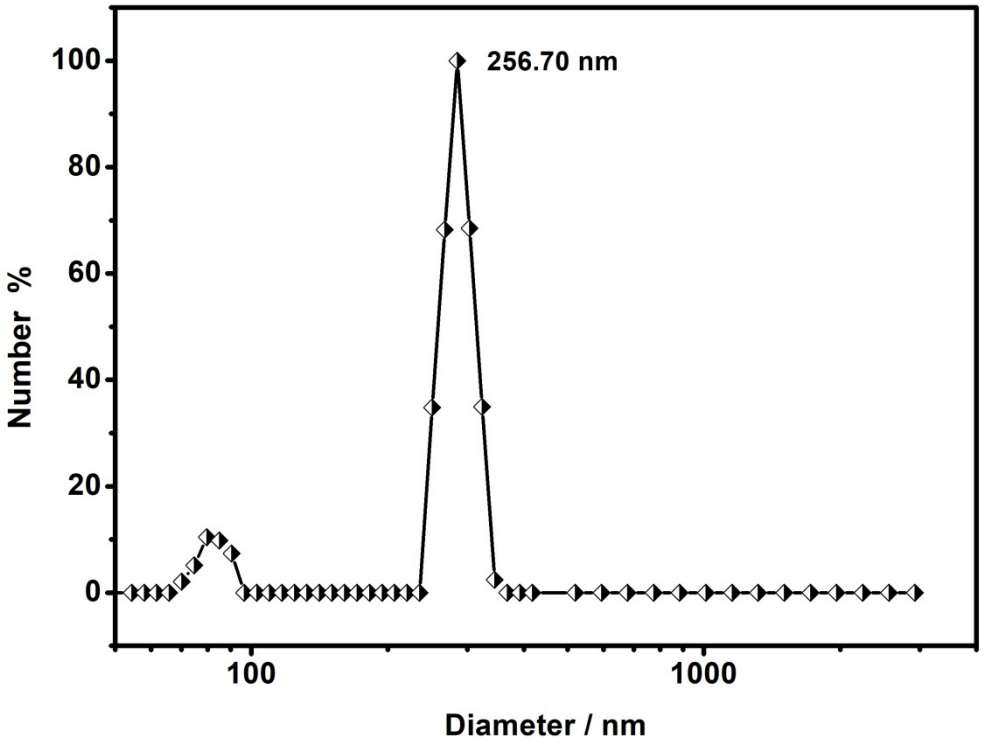

Figure S34. DLS profiles of TPA-SP_{PD}⊂CB[8].

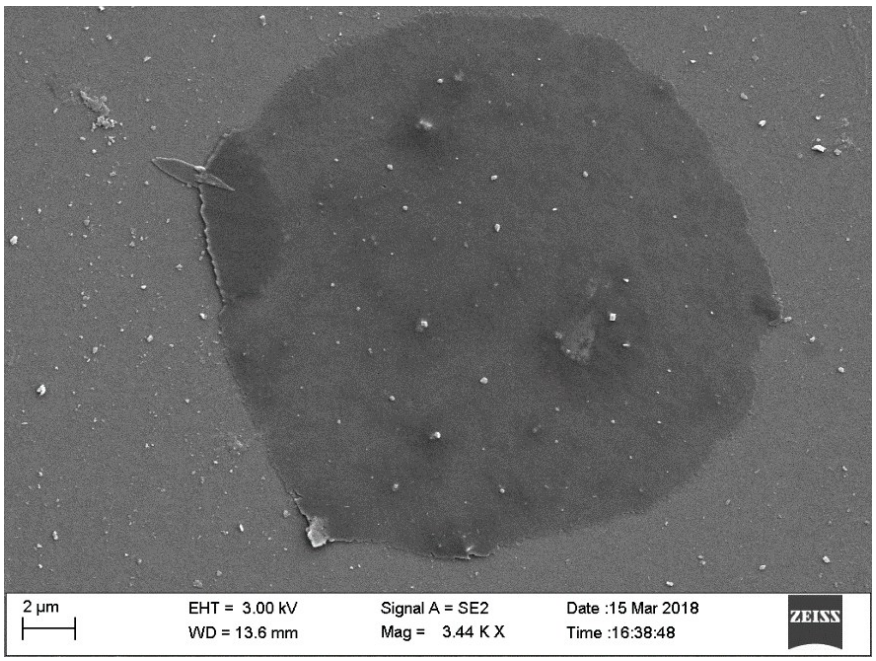

Figure S35. SEM image of TPA-SP_{PD}⊂CB[8].

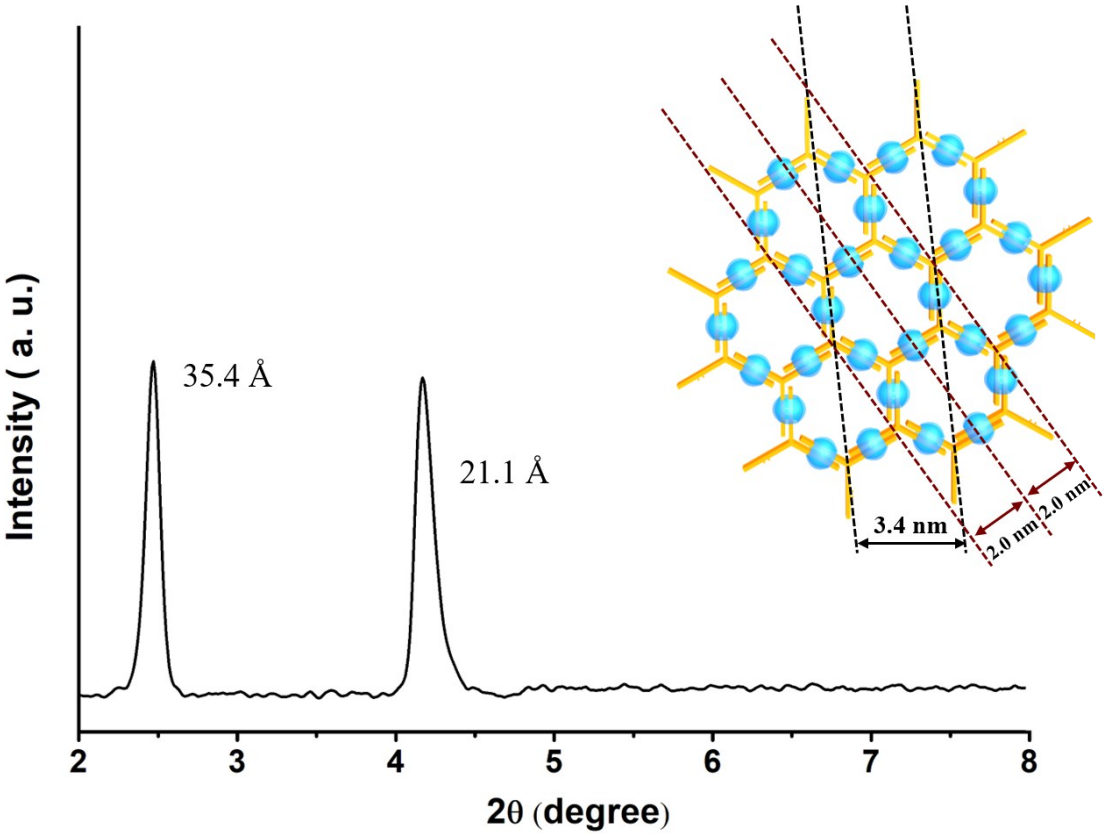

Figure S36. Grazing incidence small angle X-ray diffraction (GI-SAXS) of TPA-SP_{PD}⊂CB[8] in solid form.

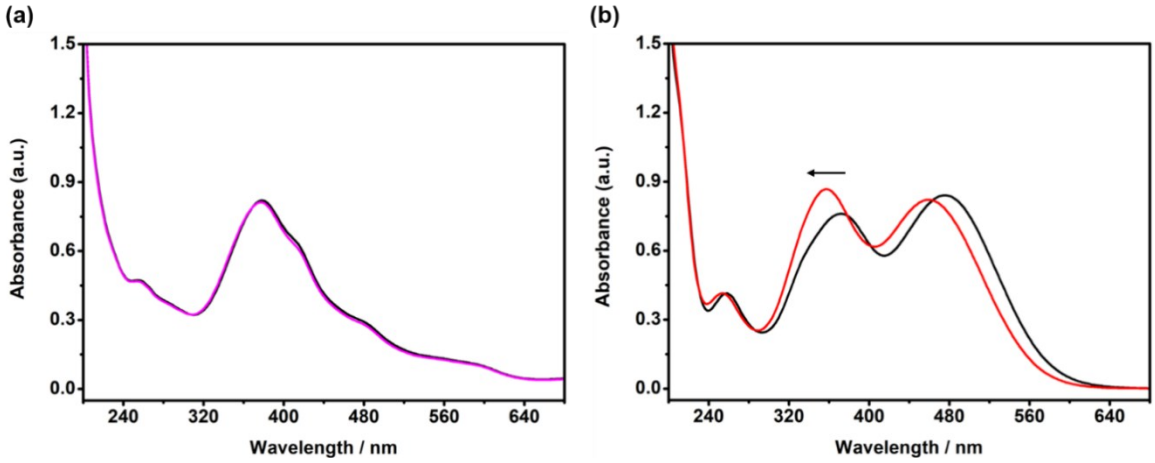

Figure S37. (a) TPA-SP_{PD}⊂CB[8] (black line) with addition of Ad-com (purple line) ([TPA-SP] = 2×10^{-5} M, [CB[8]] = 3×10^{-5} M, [Ad-com] = 3×10^{-5} M). (b) TPA-SP⊂CB[8] (black line) with addition of Ad-com (red line) ([TPA-SP] = 2×10^{-5} M, [CB[8]] = 3×10^{-5} M, [Ad-com] = 3×10^{-5} M).

There was no change in the UV/vis spectra by addition of Ad-com in the solution of TPA-SP_{PD}⊂CB[8]. However, the same operation was conducted to TPA-SP⊂CB[8], resulting in the spectrum recovering to the free TPA-SP. The experiment indicates that TPA-SP_{PD}⊂CB[8] indeed exhibited highly stability as a result of the photodimerization of SP units.

6、Characterization of C_{60}@(TPA-SP_{PD}⊂CB[8]).

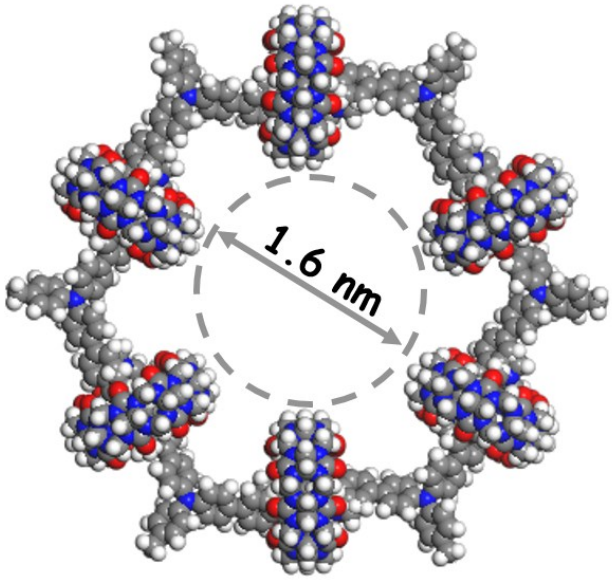

Figure S38. The diameter of available pore of TPA-SP_{PD}⊂CB[8].

The size of the simulated pore diameter is 3.4 nm, and the outer diameter of CB[8] is 1.8 nm, so that the diameter of available pore is approximate 1.6 nm, which is possible to capture C_{60}

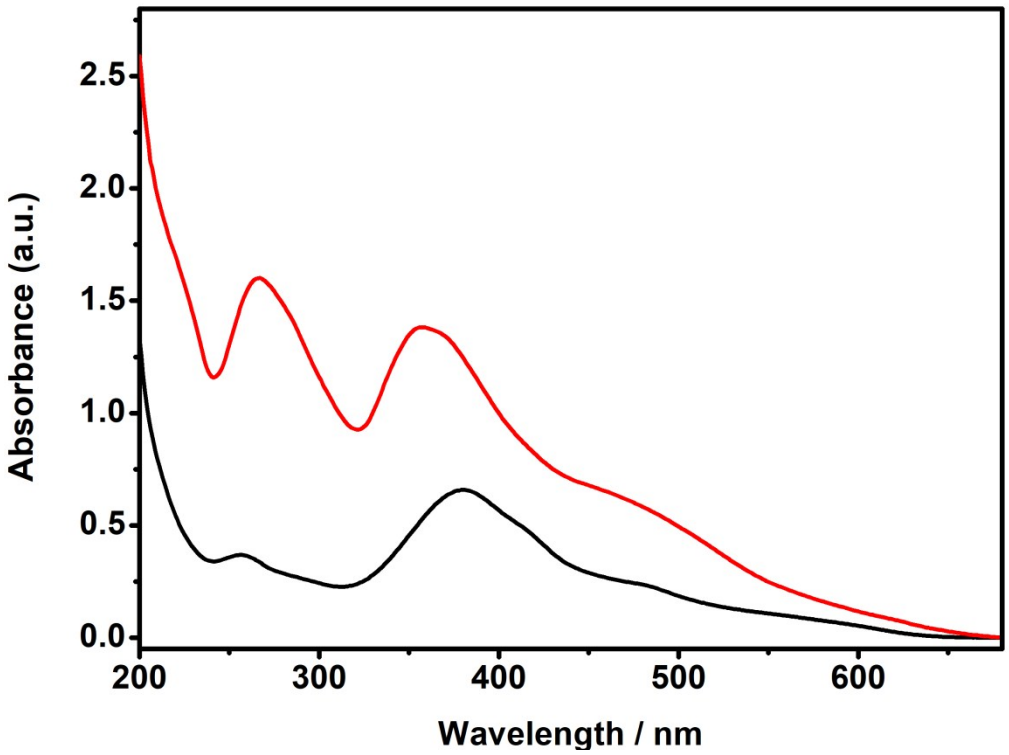

Figure S39. UV/vis spectra of TPA-SP_{PD}⊂CB[8] (black line) and C_{60}@(TPA-SP_{PD}⊂CB[8]) (red line) in water at 25 ℃.

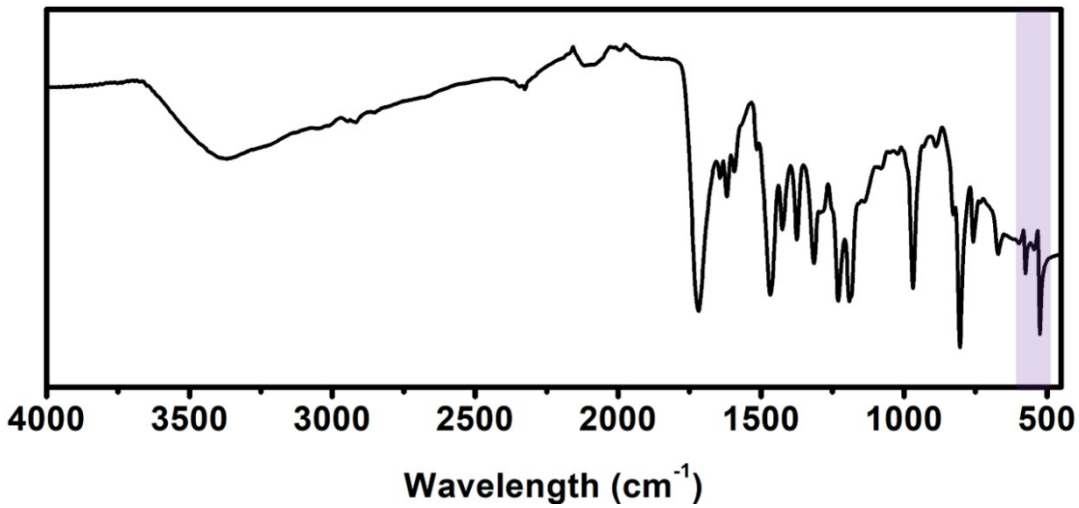

Figure S40. FTIR spectra of C_{60}@(TPA-SP_{PD}⊂CB[8]).

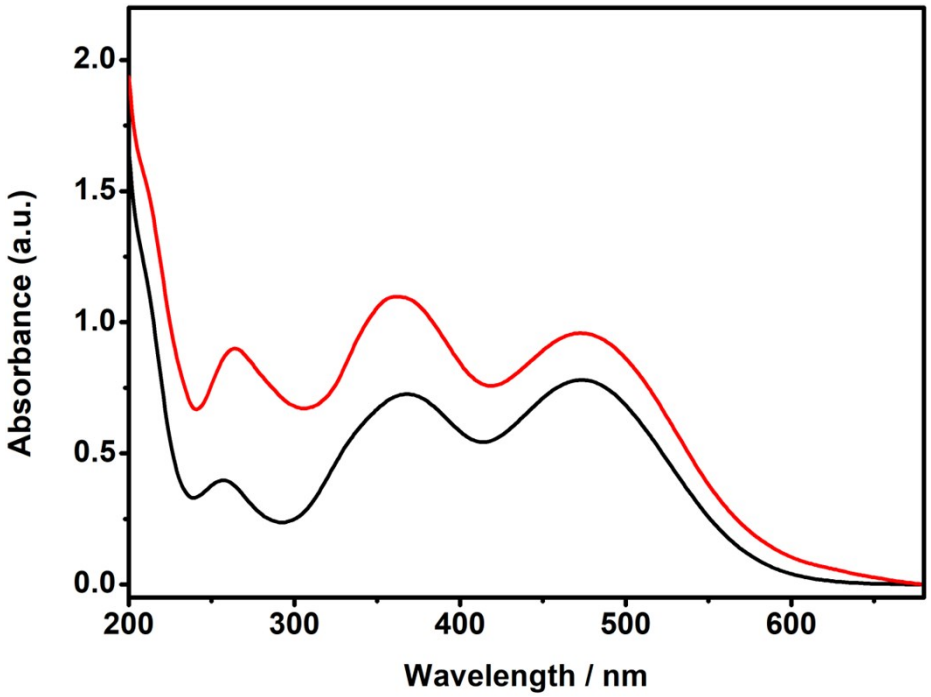

Figure S41. UV/vis spectra of TPA-SP⊂CB[8] (black line) and after capturing C_{60} (red line) in water at 25 °C.

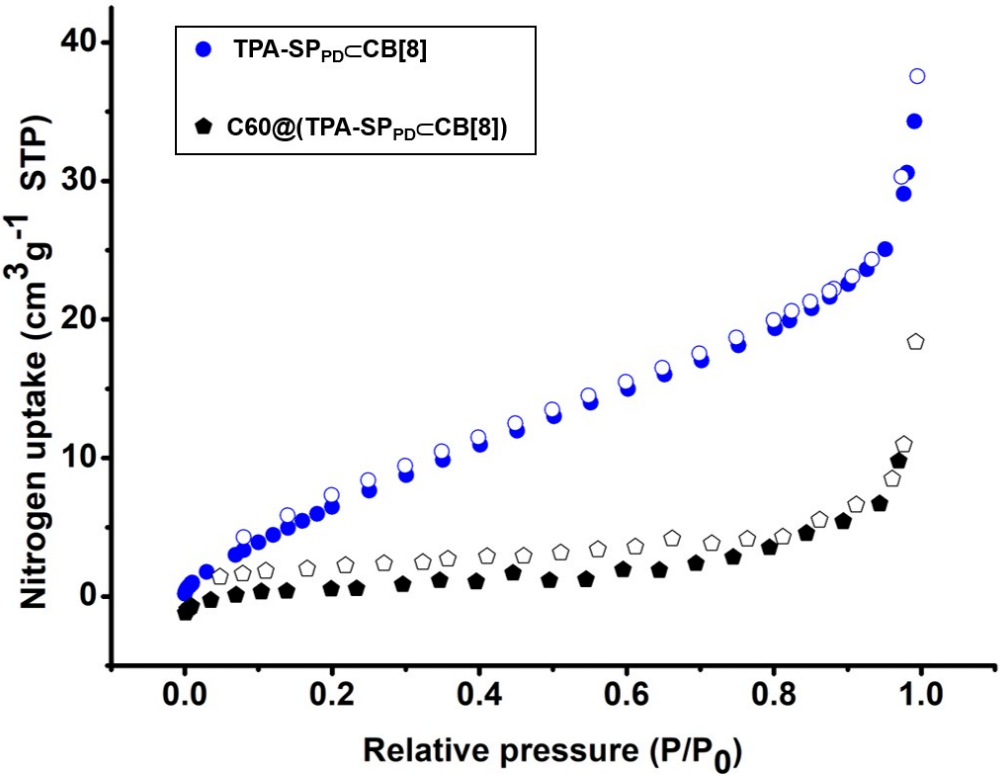

Figure S42. N_2 gas adsorption analysis of TPA-SP_{PD}⊂CB[8] (blue line) and C_{60}@(TPA-SP_{PD}⊂CB[8]) (black line).

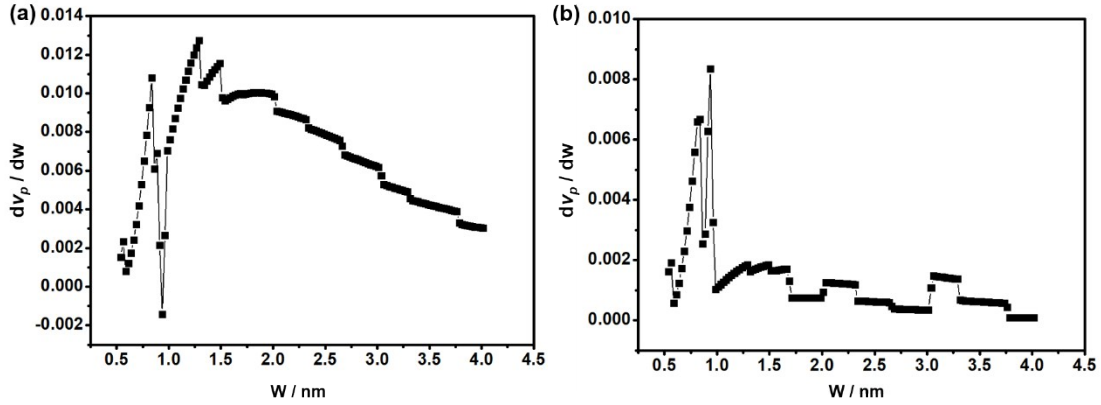

Figure S43. (a) HK-plots of TPA-SP_{PD}⊂CB[8] and (b) C_{60}@(TPA-SP_{PD}⊂CB[8]).

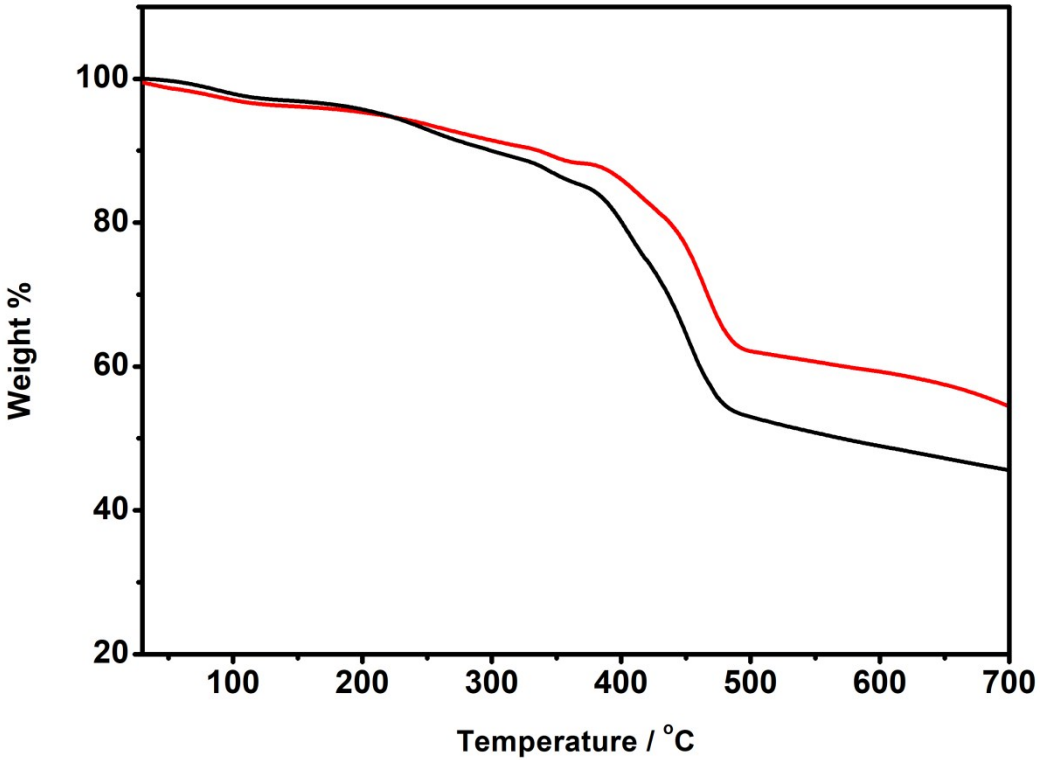

Figure S44. TGA of TPA-SP_{PD}⊂CB[8] (black line) and C_{60}@(TPA-SP_{PD}⊂CB[8]) (red line).

7、Effects of the C_{60}@(TPA-SP_{PD}⊂CB[8]) on ROS generation.

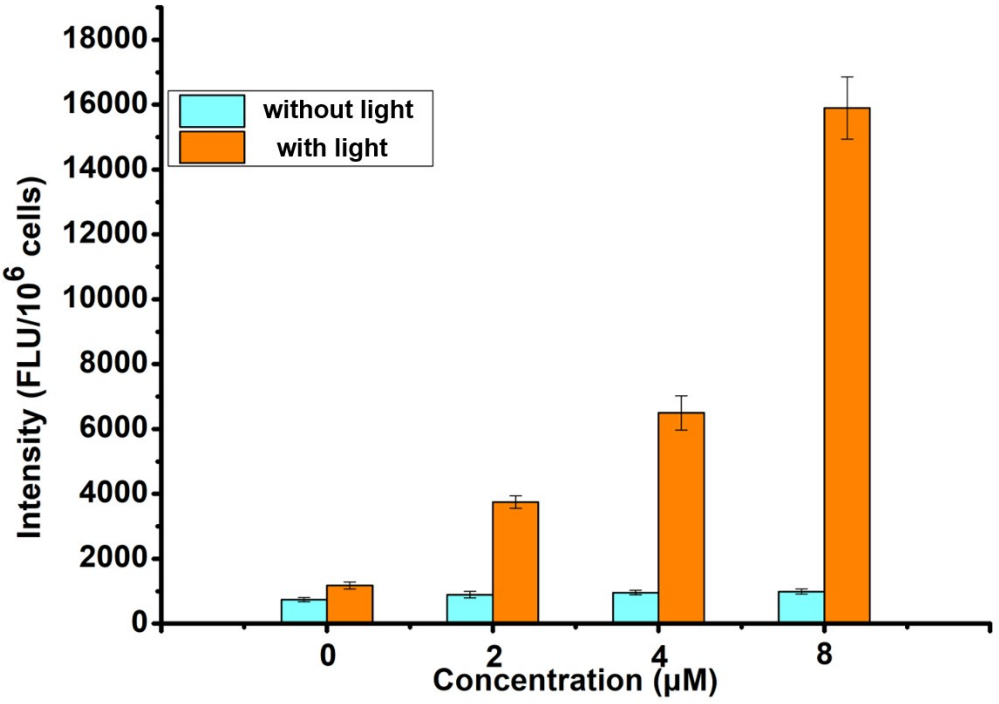

Figure S45. Effects of the C_{60}@(TPA-SP_{PD}⊂CB[8]) on ROS generation: the fluorescence intensity of DCF in A549 cells after treatment with or without irradiation with visible light for 10 min. The concentrations were calculated based on TPA-SP concentration.

8、References

S1 D. Shi, Y. Ren, H. Jiang, B. Cai, J. Lu, *Inorg. Chem.* 2012, **51**, 6498-6506.

S2 S. Liu, C. Ryspic, P. Mukhopadhyay, S. Chakrabarti, P. Y. Zavalij, L. Isaacs, *J. Am. Chem. Soc.* 2005, **127**, 15959–15967.

S3 Z. Huang, K. Qin, G. Deng, G. Wu, Y. Bai, J. F. Xu, Z. Wang, Z. Yu, O. A. Scherman, X. Zhang, *Langmuir* 2016, **32**, 12352–12360.

S4 D. Cui, J. M. MacLeod, M. Ebrahimi, D. F. Perepichka, F. Rosei, *Chem. Commun.* 2015, **51**, 16510–16513.